

Final Completion Report for R&D Projects [26.06.2018 – 25.06.2022]

Section-A: Project Details

A1. Project Title:

Understanding the role of adipose tissue remodelling in exercise induce insulin sensitivity

A2. DBT Sanction Order No., Date:

BT/PR24700/NER/95/819/2017 Dated: 26/06/2018

- A3. Name of Project Coordinator:** Dr. Suman Dasgupta
Name of Principal Investigator: Dr. Suman Dasgupta (Tezpur University)
Name of Principal Investigator: Dr. Durba Pal (IIT Ropar)
Name of Co-PI: Dr. Venkatasatishkumar Mattaparthi (Tezpur University)

A4. Institutes:

- (i) Tezpur University, Assam
(ii) Indian Institute of Technology Ropar, Punjab

A5. Address with Contact Nos. (Landline & Mobile) & Email:

Project Coordinator:

Dr. Suman Dasgupta
Department of Molecular Biology and Biotechnology,
Tezpur University, Tezpur – 784028, Napaam, Dist: Sonitpur, Assam
Phone: +91-3712-275441 (O); +91-9954332278 (M)
Email: suman.dsut@gmail.com ; suman@tezu.ernet.in

Principal Investigator (Tezpur University):

Dr. Suman Dasgupta
Department of Molecular Biology and Biotechnology,
Tezpur University, Tezpur – 784028, Napaam, Dist: Sonitpur, Assam
Phone: +91-3712-275441 (O); +91-9954332278 (M)
Email: suman.dsut@gmail.com ; suman@tezu.ernet.in

Principal Investigator (Indian Institute of Technology Ropar):

Dr. Durba Pal
Center for Biomedical Engineering,
Indian Institute of Technology Ropar,
Nangal Road, Rupnagar – 140001, Punjab
Phone: +91-1881-242211 (O); +91-8146249456 (M)
Email: durba.pal@iitrpr.ac.in

Co-PI (Tezpur University):
Dr. Venkatasatishkumar Mattaparthi
Department of Molecular Biology and Biotechnology
Tezpur University, Tezpur – 784028, Napaam, Dist: Sonitpur, Assam
Phone: +91-3712-275443 (O); +91-8811806866 (M)
Email: mvenkatasatishkumar@gmail.com

A6. Total Cost:

Rs. 74,69,992 (Rupees Seventy Four Lakhs Sixty Nine Thousand Nine Hundred and Ninety Two Only)

A7. Duration:

Four Years (26.06.2018 – 25.06.2022)

A8. Approved Objectives of the Project:

1. Investigation of exercise induced microRNAs in adipocytes and its involvement in prevention of lipid induced insulin resistance.
2. Detail study of the involvement of exercise induced microRNAs in preventing lipid induced adipocyte inflammation.
3. Evaluation of exercise induced microRNAs in lipid induced macrophage infiltration and its polarisation in the adipose tissue.

A9. Specific Recommendations made by the Task Force (if any): None

Section-B: Scientific and Technical Progress

B1. Progress made against the Approved Objectives, Targets & Timelines during the Reporting Period:

Tezpur University and IIT Ropar:

Menacing increase of type 2 diabetes mellitus (T2DM) is one of the major cause of morbidity and mortality of human beings worldwide. Pathology of this disease is characterized by the presence of insulin resistance (IR), which precedes and predicts the development of T2DM. There has been growing evidence for last few years that obesity along with physical inactivity induces chronic low-grade inflammation in adipose tissue which leads to the development of adipocyte dysfunction and IR.

It is well known that physical exercise produces beneficial effect in attenuating obesity induced insulin resistance and T2DM. Recent reports indicate that the physical exercise likely to elicit potent anti-inflammatory effect that may account for many of the salutary actions of regular exercise, however, the underlying mechanism is still not clear. Non-coding RNAs, particularly microRNAs (miRNAs), are considered as important post-transcriptional regulators of gene expression and several recent studies have revealed that they play a key role in the regulation of adipocyte function and inflammatory processes. However, till date there is no such report highlighting the role of miRNAs in exercise induced improvement of (i) adipocyte function and insulin sensitivity (ii) reduction of adipocyte inflammation and (iii) macrophage infiltration in adipose tissue and change of its polarization from Pro-inflammatory M1 to anti-inflammatory M2 state. We therefore aimed to study the role of miRNAs in exercise induced adipose tissue remodelling which could present an alternative pathway to control obesity associated adipose tissue inflammation. Since improvement of adipocyte function is the best way to counteract insulin resistance, our approach would be helpful to identify the therapeutic targets to prevent obesity induced insulin resistance and T2DM.

Adipose tissue plays a critical role in regulating both glucose and lipid homeostasis in humans. Adipose tissue contains heterogeneous cell populations mainly composed of mature adipocytes and its committed preadipocytes, mesenchymal stem cells, endothelial cells with various immune cell types including macrophages. Reports from the last few decades clearly indicate that obesity-induced hypertrophic expansion of adipose tissue is strongly correlated with the chronic low-grade inflammation implementing adipose tissue dysfunction and type 2 diabetes (T2D) pathogenesis. Moreover, the discovery of increased macrophage infiltration into the adipose tissue and proliferation of resident macrophages provided major mechanistic insight about the propagation of obesity-induced adipose tissue inflammation. It was observed that adipose tissue macrophages (ATM) comprises about 50% of the total cell population in the adipose tissue of obese subjects compared with 5-10% in lean counterparts and also the ATM content is higher in visceral than subcutaneous adipose tissue supporting the concept that visceral fat plays a major role in obesity-induced insulin resistance and T2D. Subsequent studies have demonstrated that prevention of macrophage infiltration into the adipose tissue and/or the impediment of macrophages retention within adipose tissue strikingly improved insulin sensitivity. Studies have also demonstrated that ATMs of lean mice exhibits M2 phenotype or "alternatively activated" macrophages, while in diet-induced obesity, overexpression of various pro-inflammatory genes characteristic of M1 or "classically activated" macrophages was observed. Interestingly, obesity also caused macrophage phenotypic change from an anti-inflammatory M2 to a pro-inflammatory M1 polarization state in the adipose tissue contributing to the onset of insulin resistance in mice. Recent evidence revealed a diverse population of ATMs in the obese patients that exhibits a mixed profile of several M1-M2 gene signatures, although, the prevalence of M1 population is higher than M2-like cells. All these reports provided

compelling evidence that cross-talk between inflammatory macrophages and adipocytes in the adipose tissue are paramount in the pathogenesis of obesity-induced insulin resistance and T2D. However, specific macrophage mediators or monokines involve in the cross-talk with adipocytes in obese adipose tissue triggering T2D pathogenesis are unknown and warrant further investigation. Although adipose tissue dysfunction and insulin resistance are markedly correlated with the macrophage-adipocyte cross-talk in the obese adipose tissue microenvironment, however, the causal relationship has not yet been established.

In order to test the effect of exercise mimicking condition on in vitro adipocytes, we used 3T3-L1 preadipocyte cell line in our study. 3T3-L1 preadipocytes were procured from Zenbio Inc. (Cat. No. #SP-L1-F) and cultured in 3T3-L1 preadipocyte media (Cat. No. #PM-1-L1) supplemented with 1% Penicillin-Streptomycin solution (100 µg/ml) in a humidified 5% CO₂ atmosphere at 37°C. Confluent 3T3-L1 preadipocytes were subjected to differentiation medium (Cat. No. #DM-2-L1) for 7 days. Differentiated 3T3-L1 adipocytes showing alteration of cell morphology with numerous lipid droplets stained with the oil-red O (Fig. 1A).

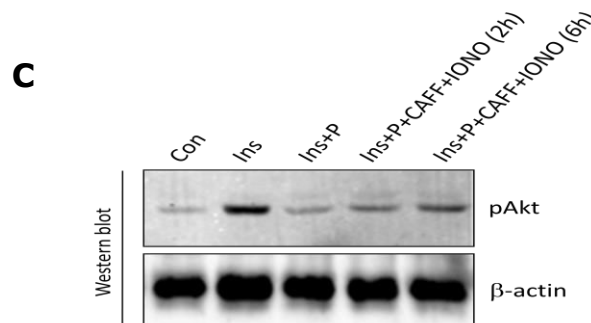
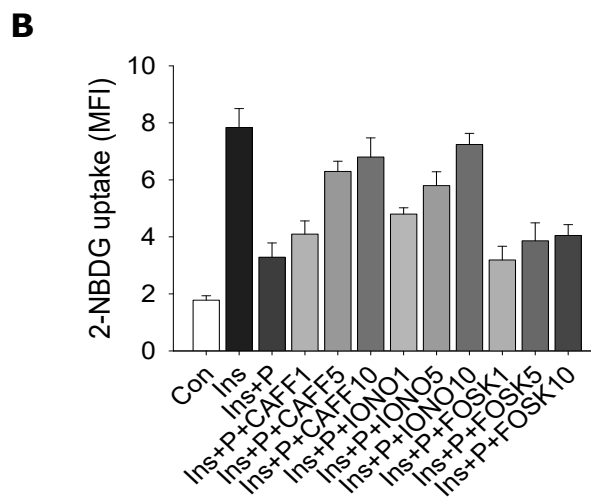
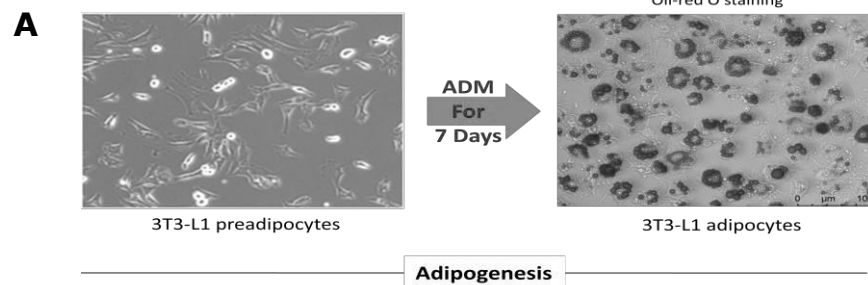


Fig. 1: (A) Conversion of 3T3-L1 preadipocytes to adipocytes (adipogenesis) by cellular differentiation for 7 days in adipocyte differentiation medium (ADM). (B) Analysis of 2-NBDG uptake by 3T3-L1 adipocytes in response to Insulin (Ins, 100 nM) or Ins + FFA (palmitate, 0.75 mM) in absence or presence of various concentrations of caffeine, ionomycin or forskolin (1, 5, 10 μ M). (C) Western blot showing pAkt (S473) abundance in 3T3-L1 adipocytes in response to insulin (Ins, 100 nM) or Ins + FFA (palmitate, 0.75 mM) in absence or presence of caffeine and ionomycin (10 μ M). β -actin was used as loading control.

Upon successful conversion, 3T3-L1 adipocytes were incubated with molecules, that mimicking the activation of exercise signaling pathways, caffeine, ionomycin and forskolin at different concentrations for 1h followed by the treatment of palmitate (0.75mM), a saturated fatty acids, for 6h. Cells were treated with insulin for 30 min followed by 10 min incubation of 2-NBDG (fluorescent labelled glucose analog) before completion of palmitate incubation. On termination of incubations, cells were harvested, lysed and fluorescent intensity was measured by Varioskan LUX Multimode Microplate Reader. Interestingly, caffeine and ionomycin treatment markedly improved the lipid-induced impairment of adipocytes glucose uptake (Fig. 1B). Forskolin treated adipocytes showed a meager effect on insulin sensitivity (Fig. 1B).

Based on this result, we selected caffeine and ionomycin for further study. To investigate the insulin signaling pathway molecules activation in response to caffeine and ionomycin, we incubated 3T3-L1 adipocytes with caffeine and ionomycin in combination for different time periods. On termination of incubations, cells were harvested, lysed in NP40 lysis buffer and supernatant was isolated for protein estimation. Cell lysates (40 μ g of protein) were subjected to 10% SDS-PAGE and transferred on to Immobilon-P PVDF membranes (Millipore, Bedford, MA) with the help of Wet/Tank Blotting System (Bio-Rad Laboratories, Hercules, CA) for Western blotting. Membranes were first blocked with 5% BSA in TBS buffer for 1h followed by the overnight incubation with primary anti phosphor-Akt or anti β -actin antibodies in a rotating shaker at 4°C. The membranes were then washed three times with TBST buffer for 10 min interval and incubated with peroxidase conjugated goat anti-rabbit secondary antibodies for 2h at room temperature. Membranes were then washed with TBST and subjected to Clarity™ Western ECL Substrate incubation for 5 min at room temperature. Protein bands were visualized and quantified in Chemidoc XRS+ System (Bio-Rad Laboratories, USA). We observed that insulin stimulated Akt phosphorylation at Ser 473 was notably impaired by palmitate incubation, however, cells treated with caffeine and ionomycin dose-dependently attenuates palmitate-induced impairment of Akt activation (Fig. 1C).

MicroRNAs (miRNAs) are considered as important post-transcriptional regulators of gene expression and several recent studies have revealed that they play a key role in the regulation of adipocyte function and inflammatory responses. miRNAs are capable to interact with partially complementary sites in the 3'UTR of mRNAs and suppress the protein synthesis via inhibition of translation or mRNA destabilization. Recent studies have determined miRNA expression profiles in M1 and M2 polarized human and murine macrophages and it has been shown differential expression of various miRNAs that regulates obesity-induced adipose tissue inflammation and insulin resistance.

Since obesity leads to adipose tissue hypoxia, we therefore investigated the expression of two well known hypoxic miRNAs, miR210 and miR126, in response to palmitate or caffeine and ionomycin coinubation. 3T3-L1 adipocytes were incubated with palmitate in absence or presence of caffeine and ionomycin followed by the extraction of RNA. The RNA quantity was measured using a NanoDrop ND-2000 spectrophotometer. RNA was reverse transcribed using iScript® cDNA synthesis kit. Quantification of miRNA expression was studied using SYBR green-based real-time PCR by using gene-specific primers. Melting curve analysis was performed after the final extension to ensure the specificity of the products. 18S rRNA was used as control. Relative expression of each gene represented as fold change over the control. Interestingly, we observed that

miR210 expression was significantly increased in response to palmitate incubation which was considerably inhibited when cells were incubated with caffeine and ionomycin (Fig. 2A). We did not notice any significant change of miR126 expression in palmitate treated cells in absence or presence of caffeine and ionomycin (Fig. 2A). Moreover, to investigate the effect of miR210 on lipid-induced adipocytes insulin resistance, we performed 2-NBDG uptake assay in miR210 inhibitor treated cells. Palmitate-induced impairment of insulin-stimulated glucose uptake was remarkably waived in miR210 inhibitor treated cells (Fig. 2B). It would be interesting to note that a marked induction of glucose uptake was observed in caffeine and ionomycin treated miR210 silenced cells (Fig. 2B). This result suggests that beside miR210, some other factors also involved in regulating insulin sensitivity in 3T3-L1 adipocytes.

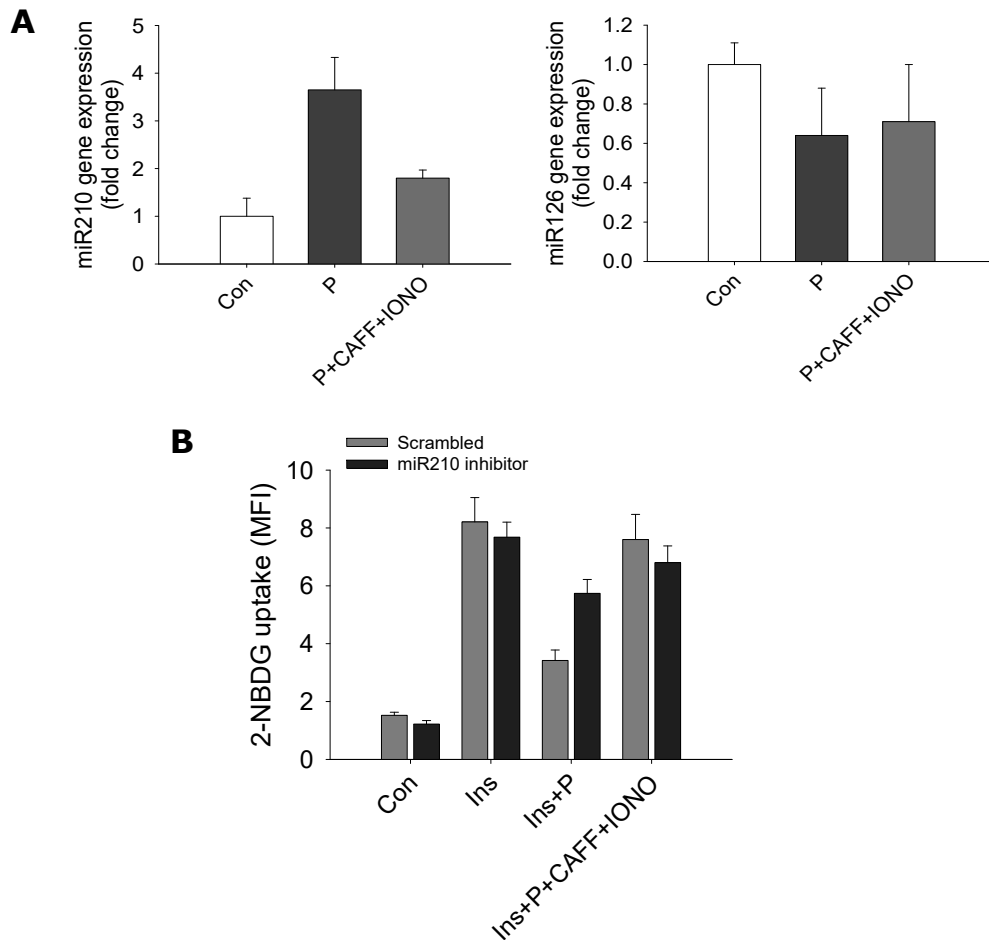


Fig. 2: (A) Real time quantitative PCR analysis showing fold change of miR210 and miR126 gene expression in 3T3-L1 adipocytes incubated without or with palmitate (0.75 mM) in absence or presence of caffeine and ionomycin (10 μ M). β -actin served as an internal control for normalization. (B) Analysis of 2-NBDG uptake in response to Insulin (Ins, 100 nM) or Ins + P (palmitate, 0.75 mM) in absence or presence of caffeine and ionomycin (10 μ M) by control inhibitor (scrambled) or miR210 inhibitor transfected 3T3-L1 adipocytes.

Since obesity leads to a macrophage phenotypic switch from an anti-inflammatory M2 to pro-inflammatory M1 state in the adipose tissue which contributes with insulin resistance and as we observed a marked induction of miR-210 in response to palmitate treatment whereas incubation of exercise mimicking chemicals notably reduced its expression improving insulin sensitivity, we therefore first examined the effect of miR-210 mimic on TNF α (pro-inflammatory) and IL-10 (anti-inflammatory) gene expression in 3T3-L1

adipocytes. Interestingly, we noticed a striking induction of TNF α gene expression along with the inhibition of IL-10 gene expression in response to miR-210 mimic treatment (Fig. 3A). Moreover, miR-210 inhibitor treatment notably prevents lipopolysaccharide (LPS)-induced inflammation as indicated by the suppression of IL-6, iNOS, and TNF- α gene expressions (Fig. 3B). All these results clearly indicate that obesity induced increased expression of miR-210 promotes macrophage migration and adipocyte inflammation. Since, exercise mimicking chemicals notably inhibit miR-210 expression and therefore, it would be a valuable target to counter the adipose tissue inflammation and insulin resistance.

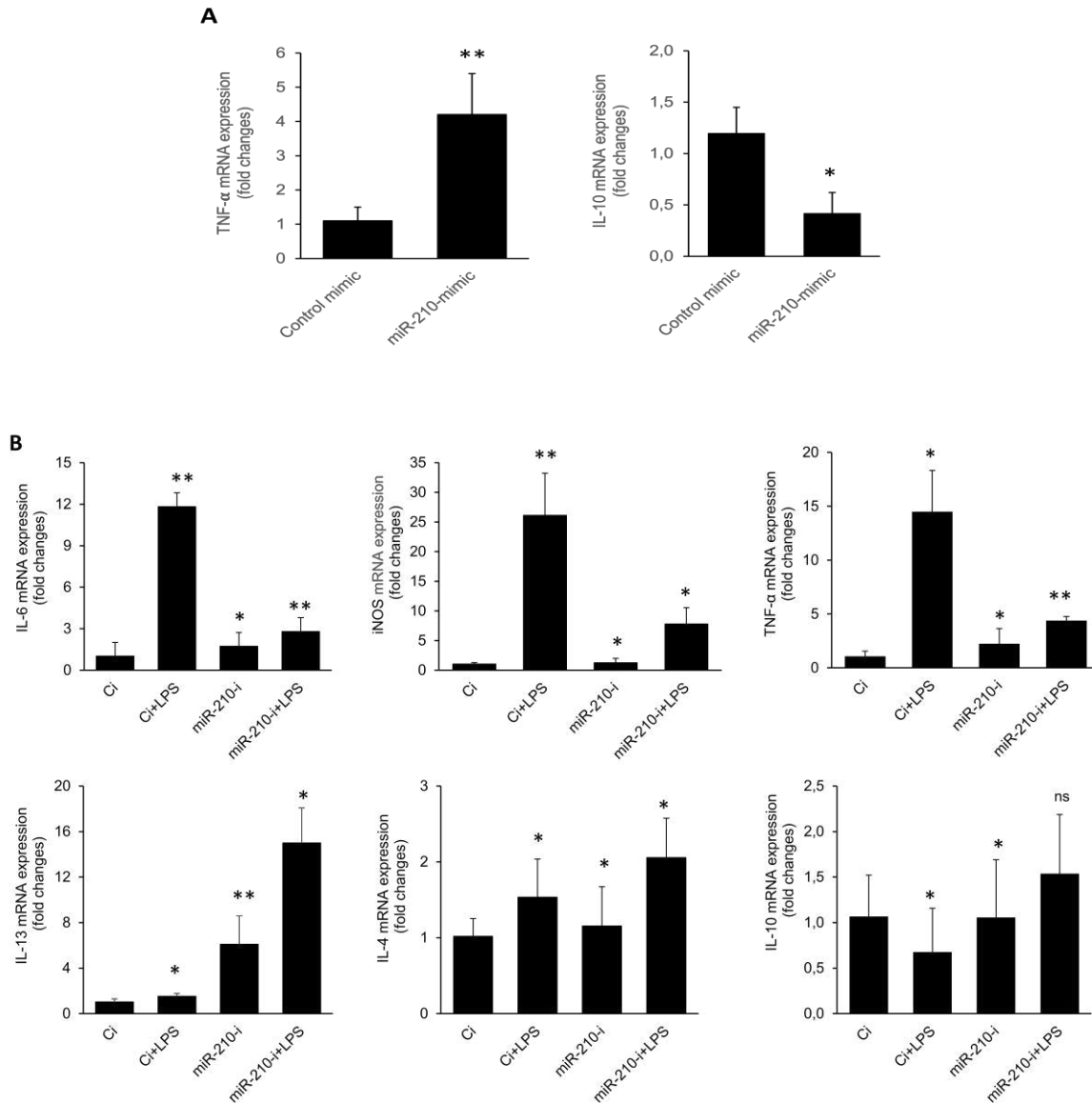


Fig. 3: (A) Real time quantitative PCR analysis showing fold change of TNF- α and IL-10 gene expression in 3T3-L1 adipocytes transfected with control mimic or miR-210 mimic. β -actin served as an internal control for normalization. (B) Real time quantitative PCR analysis showing fold change of pro-inflammatory (IL-6, iNOS, and TNF- α) and anti-inflammatory (IL-13, IL-4, and IL-10) gene expressions in control mimic or miR-210 mimic transfected adipocytes treated without or with LPS (100 nM). β -actin served as an internal control for normalization.

Our study revealed that incubation of 3T3-L1 adipocytes with exercise mimicking chemicals, ionomycin and caffeine, inhibits lipid-induced adipocyte inflammation and insulin resistance. Coincubation of caffeine and ionomycin notably stimulates insulin signalling pathway molecule Akt activation. Interestingly, we observed that palmitate incubation considerably promotes proinflammatory iNOS gene expression with a concomitant decrease of IL-10 antiinflammatory gene expression in 3T3-L1 adipocytes; however, such effect was strikingly impaired dose dependently by caffeine and ionomycin coincubation. We also noticed a significant upregulation of microRNA-210 expression in 3T3-L1 adipocytes in response to palmitate incubation which was considerably waived in caffeine and ionomycin pretreated cells. Moreover, palmitate-induced impairment of insulin-stimulated glucose uptake was notably prevented in miR-210 inhibitor treated cells. It would also be interesting to note that a notable induction of glucose uptake was observed in caffeine and ionomycin treated miR-210 silenced cells that suggest, beside miR-210, some other factors may also involved in regulating insulin sensitivity in 3T3-L1 adipocytes. Investigating the role of adipocytes miR-210 in macrophage migration, we observed that lipid-induced miR-210 expression in adipocytes notably promotes macrophage migration. Moreover, inhibition of miR-210 also waived LPS-induced adipocyte inflammation. All these results attest the involvement of miR-210 in lipid-induced adipose tissue inflammation and insulin resistance which effectively attenuated by the caffeine and ionomycin treatment and thus miR-210 could be a novel target in lipid-induced adipose tissue inflammation and insulin resistance. However, we interestingly observed that lipid incubation notably increased the expression of a monokine Cyclophilin-A (CyPA) that promotes insulin resistance. We therefore interested to examine the role of CyPA on insulin resistance.

Tezpur University:

To investigate the role of CyPA on insulin resistance *in vivo*, we prepared diet-induced obesity (DIO) in zebrafish by overfeeding (120 mg/fish/day) of commercially available feed for 4 weeks (Fig. 1A). We have found that overfeeding significantly increased body weight, and BMI in zebrafish (Fig. 1B,C) along with the enhancement of blood glucose and plasma CyPA level (Fig. 1D,E) compared to normal feeding (20 mg/fish/day). We then examined whether inhibition of CyPA by its pharmacological inhibitor TMN355 is able to mitigate obesity-induced impairment of adipose tissue dysfunction and insulin sensitivity *in vivo*, as it will be an ideal model to understand the underlying mechanism of CyPA action in implementing lipid-induced insulin resistance. To check the specificity of TMN355 action on zebrafish CyPA, we explored the protein sequence alignment of CyPA in different organisms which showed higher sequence similarity with conservation of its functional domains. Administration of TMN355 on overfed zebrafish notably decreased blood glucose level (Fig. 1D), along with the reduction of plasma CyPA level (Fig. 1E). Importantly, TMN355 administration rescued zebrafish from overfeeding-induced insulin resistance as evident from the glucose tolerance test (GTT), and insulin tolerance test (ITT) (Fig. 1F,G). Obesity-induced impairment of insulin signalling pathway markedly associated with the induction of NF- κ B-dependent inflammation that caused inhibitory serine phosphorylation, instead of tyrosine phosphorylation, of IRS-1 disrupting Akt activation. Delivery of TMN355 significantly attenuated DIO-associated inhibitory serine phosphorylation in IRS-1 and Akt inactivation in zebrafish (Fig. 1H). Moreover, DIO-associated increased activation of NF- κ B was strikingly inhibited by TMN355 treatment in zebrafish adipocytes (Fig. 1I) indicating the significance of CyPA effect on adipose tissue inflammation. All these results implicated that DIO caused increased production of CyPA which is involved in adipose tissue inflammation and insulin resistance in zebrafish.

It is now well established that the increased number of adipose tissue macrophages and its proinflammatory polarization state in obese subjects are primary inducers of chronic adipose tissue inflammation that negatively correlated with insulin sensitivity. We, therefore, embarked to ask the question of whether an increased lipid microenvironment

in obese adipose tissue may induce CyPA expression in the adipose tissue macrophages and that attenuates adipocytes insulin sensitivity. To investigate this, we first performed glucose uptake assay in 3T3-L1 adipocytes incubated with the RAW264.7 macrophages treated without or with palmitate, a saturated free fatty acid. A significant attenuation of insulin-stimulated 2-NBDG uptake was observed in adipocytes when cocultured with palmitate incubated macrophages (Fig. 2A), suggesting possible involvement of lipid-induced macrophage secretory mediator(s) on the impairment of adipocytes insulin sensitivity. Previous reports have highlighted that increased plasma levels of cyclophilin-A (CyPA) in type 2 diabetes (T2D) patients are mainly contributed by the macrophages. We found that palmitate incubation significantly increased CyPA promoter luciferase activity in RAW264.7 and THP-1 macrophages, however, it could be interesting to note that CyPA reporter activity and CyPA gene expression was not altered in 3T3-L1 adipocytes in response to palmitate treatment (Fig. 2B) indicating lipid specifically induces CyPA expression in macrophages. To confirm the macrophage originated CyPA associated with the impairment of adipocytes insulin sensitivity, CyPA silenced RAW264.7 cells were treated without or with palmitate and exposed to coculture with 3T3-L1 adipocytes for analyzing its effect on cellular glucose uptake. Interestingly, CyPA silenced macrophages treated with palmitate failed to inhibit insulin-stimulated 2-NBDG uptake by 3T3-L1 adipocytes (Fig. 2C) suggesting the participation of macrophage-derived CyPA on the attenuation of adipocytes insulin sensitivity. We performed dose and time kinetics study of palmitate on CyPA gene expression in RAW264.7 macrophages and found a dose and time dependent induction of macrophage CyPA gene expression in response to palmitate incubation (Fig. 2D). We have also found a striking increase of CyPA secretion in the culture media and the intracellular CyPA level in THP-1 macrophages in response to palmitate incubation (Fig. 2E,F). To have direct evidence in support of the role of CyPA on adipocytes insulin resistance, we incubated 3T3-L1 adipocytes with the different concentrations of CyPA for varied time periods. CyPA incubation caused dose and time dependent impairment of 2-NBDG uptake (Fig. 2G) in 3T3-L1 adipocytes. Further, CyPA-induced impairment of glucose uptake and insulin signaling pathway proteins activation was markedly inhibited by CyPA inhibitor TMN355. (Fig. 2H,I). Since JNK activation plays a key role on inhibitory IRS-1 serine phosphorylation that attenuates insulin sensitivity, we measured pJNK level and found that CyPA incubation strikingly increased JNK activation. In obese individuals, adipose tissue macrophages (ATM) are pro-inflammatory in nature showing classically activated M1 phenotype whereas ATMs of lean individuals showing anti-inflammatory signature representing alternatively activated M2 state. To examine the effect of CyPA on RAW264.7 macrophage polarization, we observed a significant induction of macrophage pro-inflammatory state in response to CyPA as indicated by the enhanced level of CD80, however, such effect was diminished by TMN355 along with the increase of anti-inflammatory marker CD206 (Fig. 2J). Collectively these results illustrated that lipid-induced upregulation of macrophage CyPA significantly promotes macrophage M1 polarization and attenuate adipocytes insulin sensitivity.

Several studies implicated the role of CyPA on cellular inflammation and since adipose tissue inflammation plays a key role in adipocyte dysfunction and insulin resistance, we decided to decipher the role of CyPA on adipocyte inflammation and its function. CyPA incubation remarkably enhanced adipocyte inflammation as exhibited by the increased expression of various pro-inflammatory cytokines genes (iNOS, TNF- α , IL-1 β , and IL-6) (Fig. 3A). Notably, suppression of CyPA by TMN355 caused inhibition of pro-inflammatory cytokines gene expressions in response to CyPA (Fig. 3A). Activation of NF- κ B transcription factor by phosphorylation and its separation from I κ B α controls the upregulation of various pro-inflammatory cytokines expression governing cellular inflammation. CyPA-induced activation of NF- κ B (Fig. 3B,C), κ B luciferase reporter activity (Fig. 3D), and NF- κ B regulated TNF- κ and IFN- γ protein expression (Fig. 3E) in 3T3-L1 adipocytes were inhibited by TMN355. Massive accumulation of infiltrated macrophages in the obese adipose tissue and the involvement of extracellular CyPA in

macrophage chemotaxis have been shown to be correlated with the chronic inflammatory states.

Adipocyte function is mainly governed by the maintenance of intricate homeostasis of preadipocyte to adipocyte differentiation or adipogenesis. To examine the role of CyPA on adipogenesis, we incubated 3T3-L1 preadipocytes with CyPA for 7 days in an adipocyte differentiation medium (ADM). Treatment of CyPA in 3T3-L1 preadipocytes affected adipogenesis as indicated by the Oil Red O staining of lipid accumulation and C16 BODIPY fluorescence, however, such attribute was prevented when co-treated with TMN355 (Fig. 4A,B). Since PPAR- γ and C/EBP- β function as key transcriptional activators regulating adipocyte differentiation through the induction of different adipogenic gene expressions such as FABP-4, and Glut-4, we evaluated the expression profile of these markers in response to CyPA. A striking reduction of PPAR- γ , C/EBP- β , and FABP-4 gene expression in CyPA incubated 3T3-L1 cells were notably rescued by TMN355 treatment (Fig. 4C). Additionally, the subdued level of FABP-4 and Glut-4 proteins in 3T3-L1 cells in response to CyPA was significantly inhibited by TMN355 incubation (Fig. 4D). There was no change in de novo lipogenesis as indicated by triglyceride release from adipocytes (Fig. 4E) and the lipogenic markers gene expression such as Acetyl-CoA carboxylase (ACC), and sterol regulatory element-binding protein-1c (SREBP-1c) (Fig. 4F), although a considerable downregulation of lipoprotein lipase (LPL) gene expression was observed in CyPA treated cells (Fig. 4F). Together, these experiments demonstrated that CyPA-induced impairment of adipogenesis and lipid uptake may be responsible for adipocyte dysfunction.

Accumulating evidence indicated CD147 as a cell surface signaling receptor of extracellular CyPA which mediates its chemotactic activity toward a variety of immune cells. A report in this direction implicated that Pro³⁰⁹ and Gly³¹⁰ residues in CD147 are critical for CyPA mediated signaling. We, therefore, investigated the role of CyPA-CD147 signaling on adipogenesis and adipocyte inflammation. For this, wild-type CD147 or mutant CD147 (P309A and G310A) plasmid was cotransfected with either PPRE-luc or κ B-luc plasmid followed by the incubation of CyPA in 3T3-L1 preadipocytes for 7 days in ADM. CyPA-induced impairment of PPRE-luciferase activity and the induction of κ B-luciferase activity was significantly waived in 3T3-L1 cells expressing mutated CD147 (P309A and G310A) (Fig. 5A,B). This was further validated by gene expression analysis of adipogenic and inflammatory markers, as CyPA-induced inhibition of adipogenic PPAR- γ and C/EBP- β gene expression and the induction of pro-inflammatory cytokines TNF- α and IL-1 β gene expression were markedly prevented in 3T3-L1 cells expressing mutated CD147 (P309A and G310A) (Fig. 5C,D). These data strongly suggest the participation of P309/G310 residues of CD147 plays a key role in CyPA-induced impairment of adipogenesis and induction of adipocyte inflammation.

However, to explore the underlying mechanism of CyPA action downstream of CD147, we used pharmacological inhibitors of NF- κ B pathway (Bay 11-7085) and Wnt signaling pathway (IWR-1-endo) as these signaling cascades were involved in cellular inflammation and adipocyte differentiation, respectively. Although treatment of NF- κ B pathway inhibitor significantly diminished CyPA effected upregulation of pro-inflammatory cytokines gene expression and downregulation of adipogenic markers gene expression (Fig. 6A), however, inhibition of Wnt signaling only rescued CyPA mediated adipogenic markers expression without any notable changes in pro-inflammatory cytokines expression (Fig. 6B,C). Depending on cell types and disease pathogenicity, both positive and negative regulation of Wnt/ β -catenin by NF- κ B was reported previously. It has been reported that NF- κ B indirectly regulates the Wnt/ β -catenin pathway either through Leucine zipper tumor suppressor 2 (LZTS2), or by SMAD ubiquitination regulatory factor 1 (Smurf1) and Smurf2 that interact with β -catenin and regulates its stability or degradation affecting transcriptional activity. Investigating this aspect, we successfully demonstrated that CyPA incubation significantly downregulates

LZTS2 gene expression without any noticeable changes in Smurf1 and Smurf2 gene expression. By contrast, subdued expression of LZTS2 in response to CyPA incubation was considerably prevented by Bay 11-7082 treatment in 3T3-L1 adipocytes (Fig. 6D). We conclude that CyPA-CD147 signaling-mediated NF- κ B activation directly promotes adipocyte inflammation and indirectly attenuates adipogenesis through the downregulation of LZTS2.

To examine the role of palmitate-induced CyPA on adipose tissue inflammation and insulin resistance *in vivo*, we infused palmitate intraperitoneally in wild-type BL/6 mice followed by the intraperitoneal administration of CyPA inhibitor TMN355. Palmitate infusion markedly augments serum CyPA level which was significantly waived by TMN355 (Fig. 7A). Increased accumulation of adipose tissue macrophages (ATMs) in response to palmitate infusion was notably rescued by TMN355 administration as indicated by flow cytometric analysis of F4/80+CD11b+ cells in the stromal vascular fraction of adipose tissue (Fig. 7B) and immunohistochemical analyses of F4/80 level in the visceral adipose tissue (Fig. 7C). Moreover, TMN355 delivery significantly relinquished palmitate-induced enhancement of TNF α and IL-6 proinflammatory cytokines levels (Fig. 7D). Inhibition of palmitate-mediated adipose tissue inflammation by TMN355 was coincided with the amelioration of glucose intolerance and insulin insensitivity as evident from the glucose tolerance test (Fig. 7E), homeostasis model assessment–insulin resistance (HOMA-IR) scores (Fig. 7F) and the inhibitory or stimulatory phosphorylation of the insulin-signaling molecules IRS-1 and Akt, respectively (Fig. 7G). All these results indicate that palmitate-infusion in mice notably upregulates CyPA expression which associated with the adipose tissue inflammation and insulin resistance.

For the *in vivo* validation about the participation of CD147 in mediating CyPA effect on adipocyte dysfunction and insulin resistance, we infused CyPA in mice and then delivered anti-CD147 antibody (CD147-Ab) through intraperitoneal route. Similar to TMN355 effect on palmitate-induced ATMs accumulation, we have found that CD147-Ab delivery significantly prevented CyPA-induced macrophage migration as evident from F4/80+CD11b+ cell population in the stromal vascular fraction of adipose tissue (Fig. 8A) and the F4/80 level in the visceral adipose tissue (Fig. 8B). However, it could be interesting to note that CyPA effect on adipose tissue macrophage migration was more pronounced than palmitate infusion. Moreover, delivery of CD147-Ab notably waived CyPA-induced upregulation of serum level of TNF α and IL-6 proinflammatory mediators (Fig. 8C). Since we have found that CyPA-CD147 signaling impairs the adipogenesis process in the *in vitro* condition, we explored the gene expression profile of two key adipogenesis regulators PPAR γ and C/EBP β in mice infused with CyPA without or with CD147-Ab. Delivery of CD147-Ab in mice significantly restored CyPA-induced attenuation of PPAR γ and C/EBP β gene expression (Fig. 8D). Furthermore, targeted blocking of CD147 by delivering CD147-Ab in mice rescued from CyPA-induced glucose intolerance (Fig. 8E), and insulin sensitivity as indicated by the HOMA-IR scores (Fig. 8F), and insulin signalling pathway molecules IRS-1 and Akt inactivation and activation, respectively. These results provide clear evidence that CyPA directly associated with the impairment of adipocyte functions and insulin sensitivity in the *in vivo* condition.

Figure 1

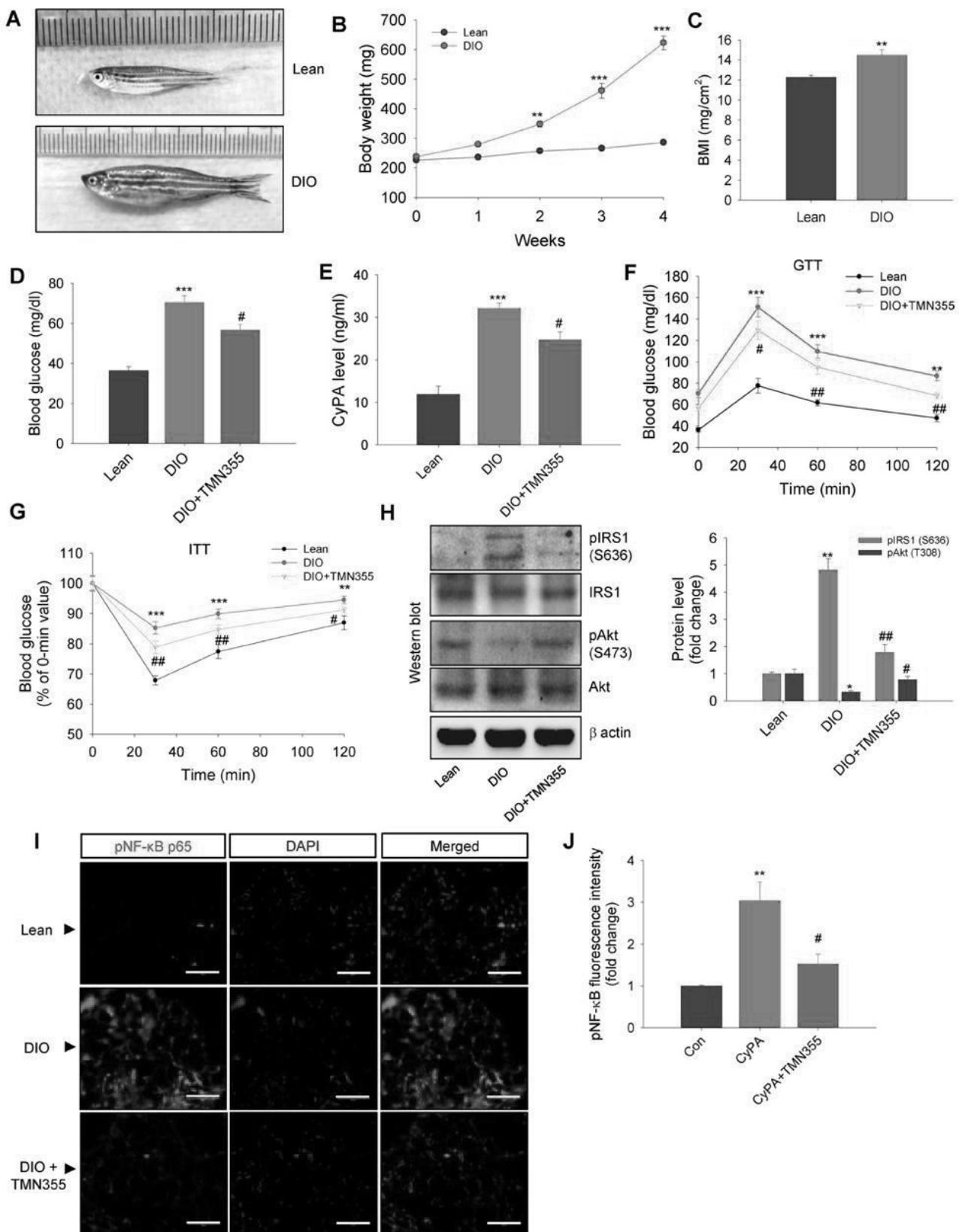


Fig. 1 CyPA induces insulin resistance and type 2 diabetes in obese zebrafish. **A–C** Photographic images (**A**), body weight (**B**), BMI (**C**) value of lean and diet-induced obese (DIO) zebrafish ($n=4$). **D**, **E** Blood glucose level (**D**), and ELISA of plasma CyPA level (**E**) of lean- or DIO- or DIO plus TMN355 administrated zebrafish ($n=3$). **F–H** Insulin resistance was determined by measuring oral glucose tolerance test (**F**), intraperitoneal insulin tolerance test (**G**), and western blot analyses of insulin-signaling pathway molecules activation and inactivation (**H**) in these zebrafish ($n=12$). **I**, **J** Immunohistochemistry images of pNF-κB (**I**) and its quantification (**J**) in the adipose tissue from lean- or DIO- or DIO plus TMN355 administrated zebrafish ($n=3$). Scale bar, 100 μm. Each value represent as mean ± SEM, *** $p < 0.001$, ** $p < 0.01$, * $p < 0.05$ vs lean; ### $p < 0.001$, ## $p < 0.01$, # $p < 0.05$ vs DIO

Figure 2

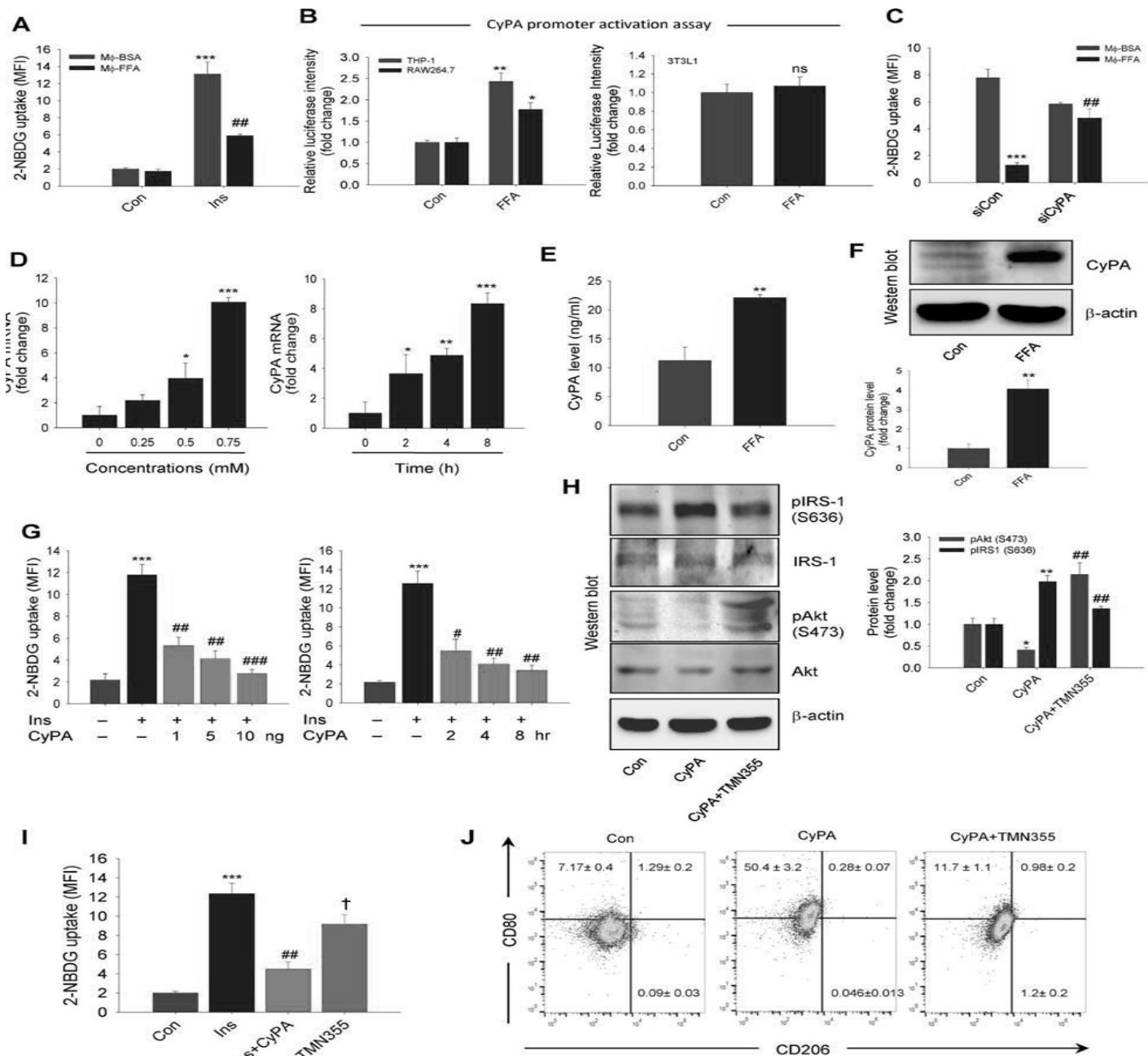


Fig. 2 Lipid incubation stimulates macrophage CyPA expression which induces insulin resistance in 3T3-L1 adipocytes. **A** Determination of insulin-stimulated 2-NBDG uptake by 3T3-L1 adipocytes in response to the conditional media of RAW264.7 macrophage treated without or with a saturated free-fatty acid palmitate (FFA, 0.75 mM) for 8 h, *** $p < 0.001$ vs Mφ-BSA-Con, ## $p < 0.01$ vs Mφ-BSA-Ins. **B** CyPA promoter activity was measured in RAW264.7 macrophages, THP-1 macrophages, and 3T3-L1 adipocytes transfected with CyPA promoter luciferase reporter plasmid followed by the incubation of palmitate (0.75 mM) for 8 h, ** $p < 0.01$, * $p < 0.05$ vs Con, *ns* non-significant. **C** Analysis of insulin-stimulated 2-NBDG uptake by 3T3-L1 adipocytes in response to the conditional media obtained from control siRNA or CyPA siRNA-transfected cells treated without or with palmitate (0.75 mM) for 8 h, *** $p < 0.001$ vs Mφ-BSA-siCon, ## $p < 0.05$ vs Mφ-FFA-siCon. **D** RT-qPCR analysis of CyPA gene expression in RAW264.7 macrophages treated with different concentrations of palmitate (0, 0.25, 0.50, and 0.75 mM) for 8 h or 0.75 mM of palmitate for varied time periods (0, 2, 4, 8 h). 18 s RNA was used as loading control, *** $p < 0.001$, ** $p < 0.01$ * $p < 0.05$ vs Con. **E** ELISA showing CyPA secretion from THP-1 macrophages treated without or with palmitate (0.75 mM) for 8 h, ** $p < 0.01$ vs Con. **F** Western blot (upper) and its quantification (lower) showing abundance of CyPA in THP-1 macrophages in response to palmitate (0.75 mM) incubation for 8 h. β-Actin was used as loading control, ** $p < 0.01$ vs Con. **G** Dose- and time-dependent effect of CyPA on insulin-stimulated 2-NBDG uptake by 3T3-L1 adipocytes, *** $p < 0.001$ vs Con; ### $p < 0.001$, ## $p < 0.01$, # $p < 0.05$ vs Ins. **H** Western blot (left) and its quantification (right) showing pAkt (S473) and pIRS1 (S636) abundance in 3T3-L1 adipocytes treated without or with CyPA (10 ng/ml) in the absence or presence of CyPA inhibitor TMN355 (1 μM) for 8 h. β-Actin was used as loading control, ** $p < 0.01$, * $p < 0.05$ vs Con; ## $p < 0.01$ vs CyPA. **I** Determination of insulin-stimulated 2-NBDG uptake by 3T3-L1 adipocytes in response to CyPA (10 ng/ml) treated without or with TMN355 (1 μM) for 8 h, *** $p < 0.001$ vs Con, ## $p < 0.01$ vs Ins, † $p < 0.05$ vs Ins+CyPA. **J** Flow cytometric analysis of CD80 and CD206 levels in RAW264.7 macrophages treated without or with CyPA (10 ng/ml) in the absence or presence of TMN355 (1 μM) for 8 h. All experiments were performed in triplicate. Each value is the mean ± SEM of three independent experiments.

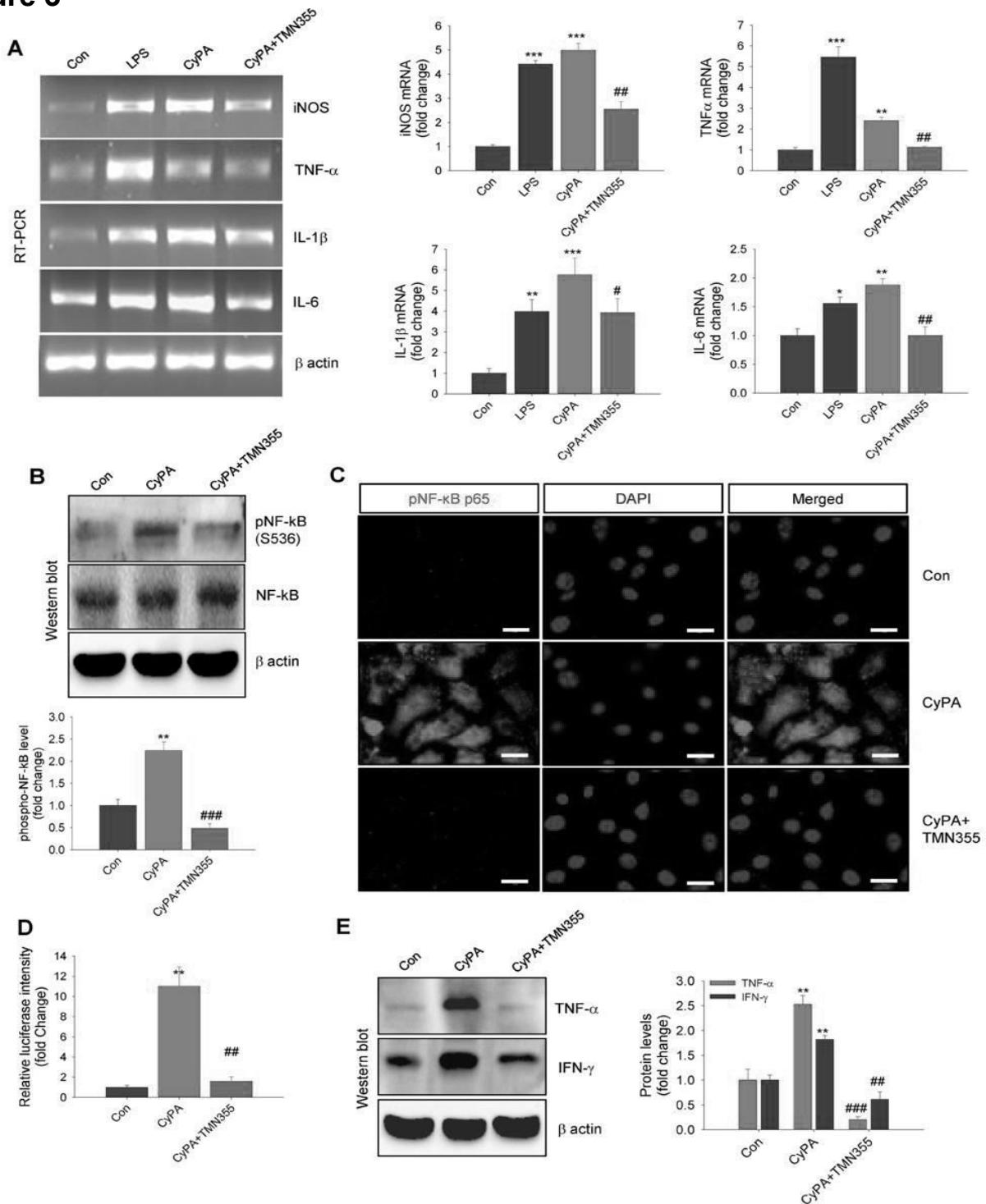
Figure 3

Fig. 3 CyPA stimulates adipocyte inflammation. **A** RT-PCR analysis (left) and its quantification (right) of iNOS, TNF- α , IL-1 β and IL-6 gene expressions in 3T3-L1 adipocytes treated without or with CyPA (10 ng/ml) in the absence or presence of TMN355 (1 μ M). LPS (100 ng/ml) was used as positive control. β -Actin serves as loading control. **B** Western blot (upper) and its quantification (lower) showing pNF- κ B abundance in 3T3-L1 adipocytes incubated without or with CyPA (10 ng/ml) in the absence or presence of TMN355 (1 μ M) for 8 h. β -Actin was used as loading control. **C** Immunofluorescence images showing pNF- κ B level in 3T3-L1 adipocytes incubated without or with CyPA (10 ng/ml) in the absence or presence of TMN355 (1 μ M) for 8 h. Scale bar, 20 μ m. **D** 3T3-L1 adipocytes transfected with κ B promoter luciferase plasmid was incubated without or with CyPA (10 ng/ml) in the absence or presence of TMN355 (1 μ M) for 8 h. On termination of incubations, cells were lysed and luciferase activity was measured by multimode reader. **E** Western blots (left) and their quantifications (right) showing TNF- α , and IFN- γ abundance in 3T3-L1 adipocytes incubated without or with CyPA (10 ng/ml) in the absence or presence of TMN355 (1 μ M) for 8 h. β -Actin was served as loading control. All experiments were performed in triplicate. Each value is the mean \pm SEM of three independent experiments, *** p < 0.001, ** p < 0.01, * p < 0.05 vs Con; ### p < 0.001, ## p < 0.01, # p < 0.05 vs CyPA

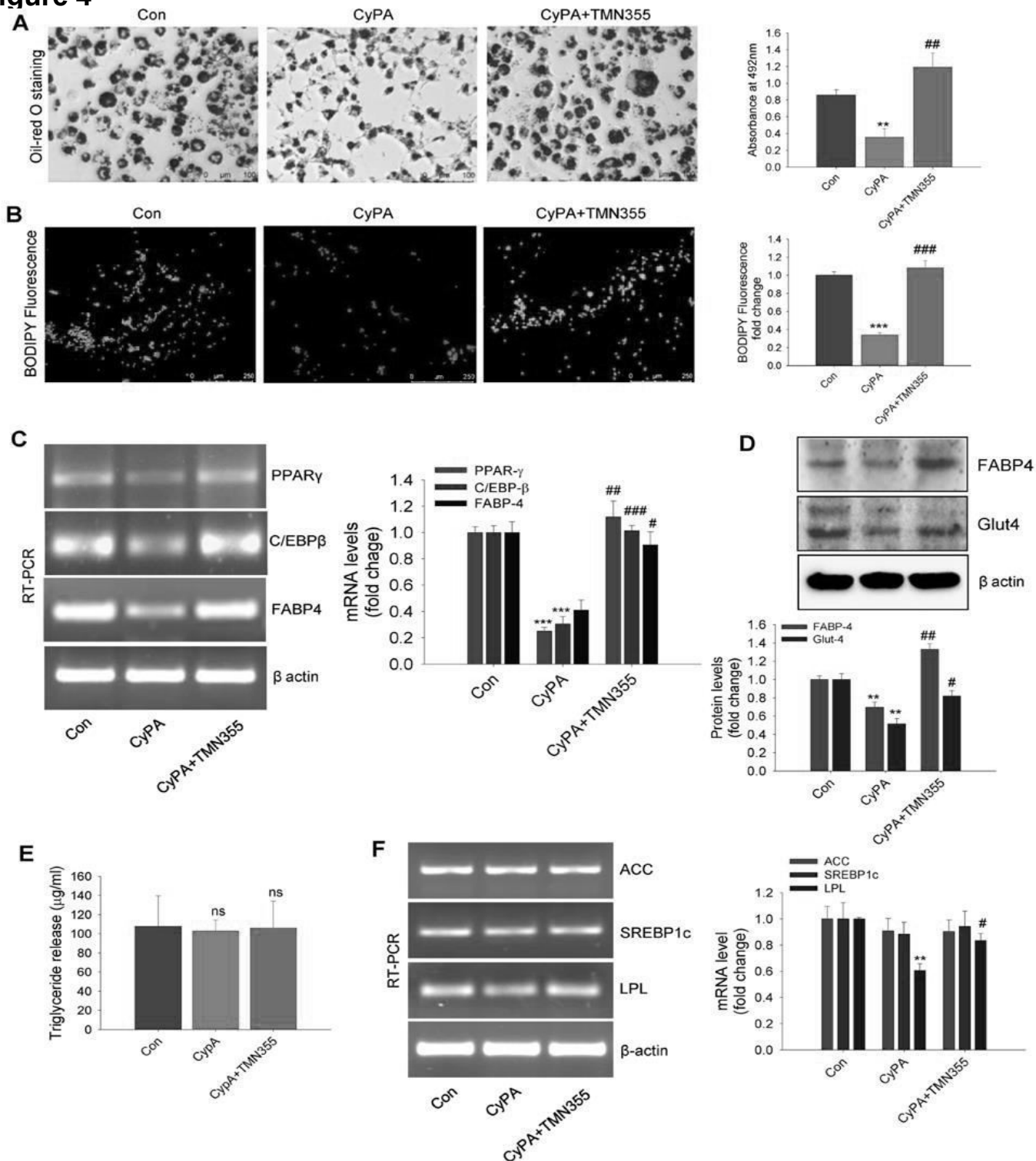
Figure 4

Fig. 4 CyPA-induced adipocyte dysfunction was prevented by TMN355. **A, B** Oil-Red O staining images (left) and the estimation of lipid contents (right) (**A**), and C16 BODIPY fluorescence images (left) and its quantifications (right) (**B**) representing 3T3-L1 adipocyte differentiation in response to CyPA (10 ng/ml) incubation without or with TMN355 (1 μM) for 7 days in the presence of adipocyte differentiation medium (ADM). Scale bar, 100 μm (**A**) and 250 μm (**B**). **C, D** RT-PCR analysis (left) and its quantification (right) of PPAR-γ, C/EBP-β, and FABP-4 gene expressions (**C**) and Western blot images (upper) and its quantifications (lower) showing abundance of FABP-4 and Glut-4 proteins (**D**) in 3T3-L1 cells treated without or with CyPA (10 ng/ml) in the absence or presence of TMN355 (1 μM) for 7 days in ADM. β-Actin was served as loading control for RT-PCR and Western blotting. **E** Lipogenesis was measured by the estimation of triglyceride release into the cell culture medium of 3T3-L1 cells treated without or with CyPA (10 ng/ml) in the absence or presence of TMN355 (1 μM) for 7 days in ADM. **F** RT-PCR analysis (left) and its quantification (right) showing abundance of ACC, SREBP1c, and LPL mRNA levels in 3T3-L1 cells treated without or with CyPA (10 ng/ml) in the absence or presence of TMN355 (1 μM) for 7 days in ADM. β-Actin was used as loading control. All experiments were performed in triplicate. Each value is the mean ± SEM of three independent experiments, ****p* < 0.001, ***p* < 0.01 vs Con; ###*p* < 0.001, ##*p* < 0.01, #*p* < 0.05 vs CyPA; *ns* non-significant

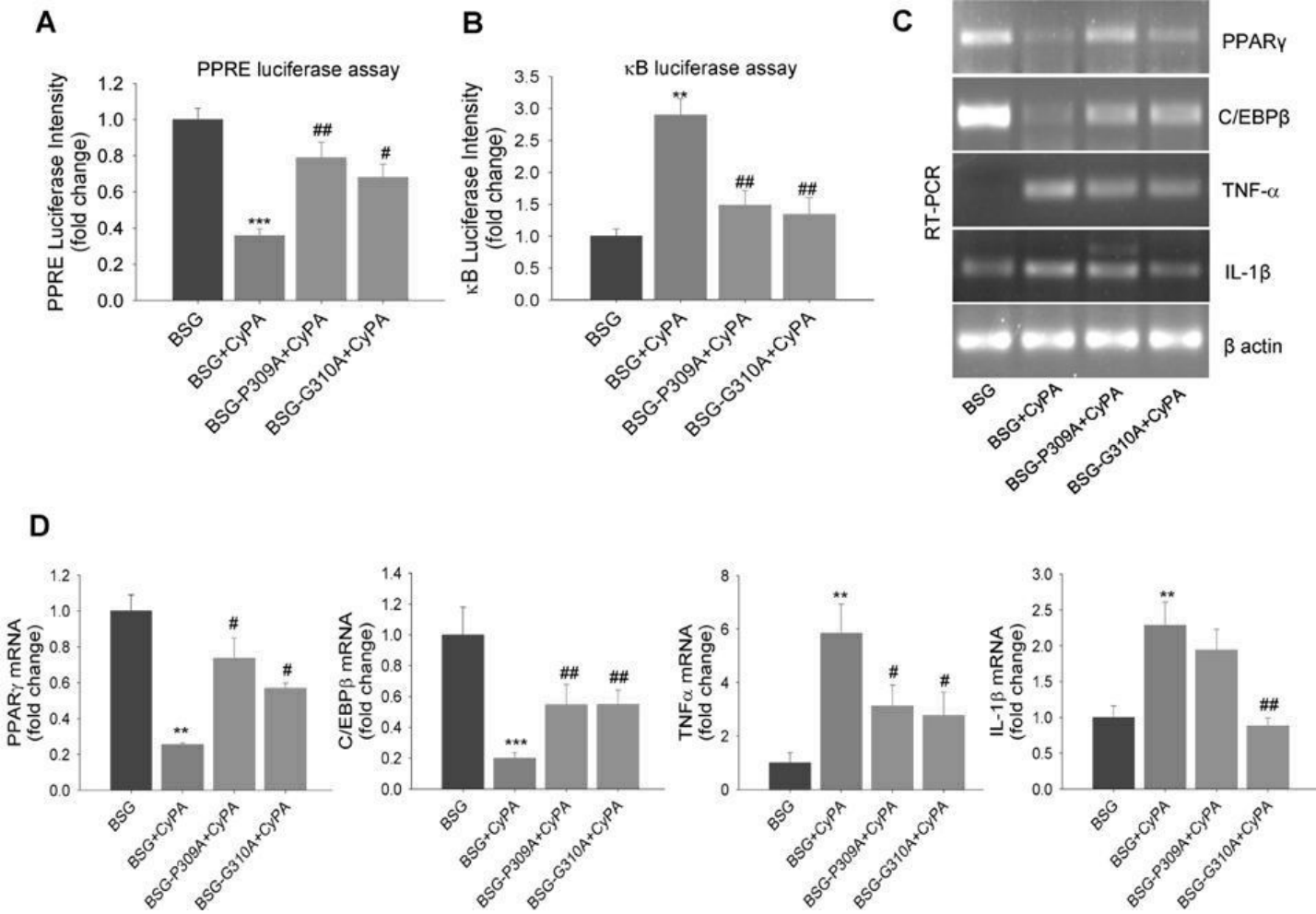
Figure 5

Fig. 5 CD147 mediates CyPA-induced adipocyte inflammation and its dysfunction. **A, B** Wild-type or mutated CD147 (basigin, BSG) plasmids (P309A and G310A) were cotransfected with PPRE promoter luciferase plasmid (**A**) or κ B promoter luciferase plasmid (**B**) in 3T3-L1 adipocytes and incubated without or with CyPA (10 ng/ml) for 8 h. On termination of incubations, cells were lysed and luciferase activity was measured by a multimode reader. **C, D** RT-PCR

analysis (**C**) and its quantification (**D**) of PPAR- γ , C/EBP- β , TNF- α , and IL-1 β gene expressions in wild-type or mutated CD147 plasmid transfected 3T3-L1 adipocytes treated without or with CyPA (10 ng/ml) for 8 h. β -Actin was used as loading control. All experiments were performed in triplicate. Each value is the mean \pm SEM of three independent experiments, *** p < 0.001, ** p < 0.01 vs BSG, ## p < 0.01, # p < 0.05 vs BSG+CyPA

Figure 6

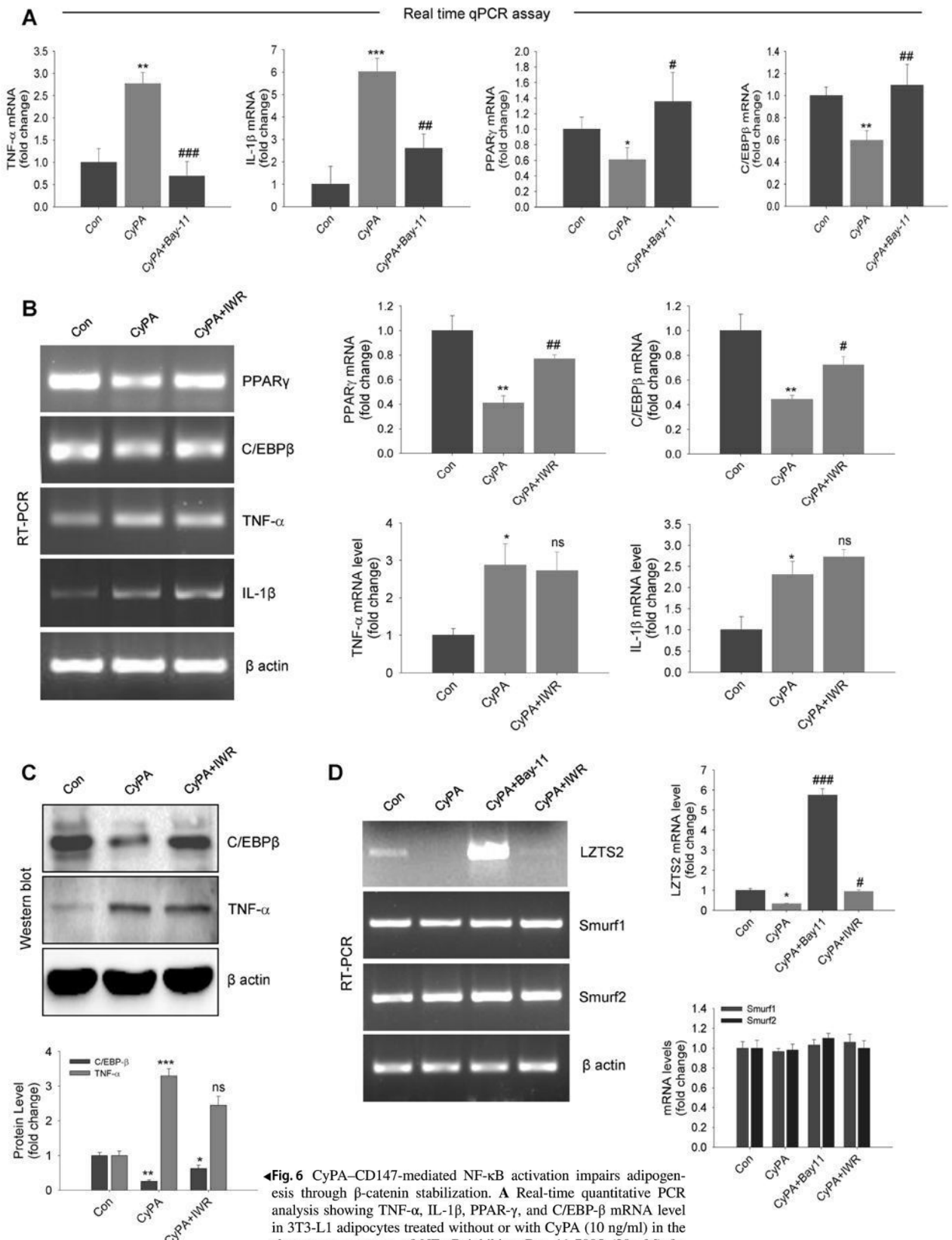
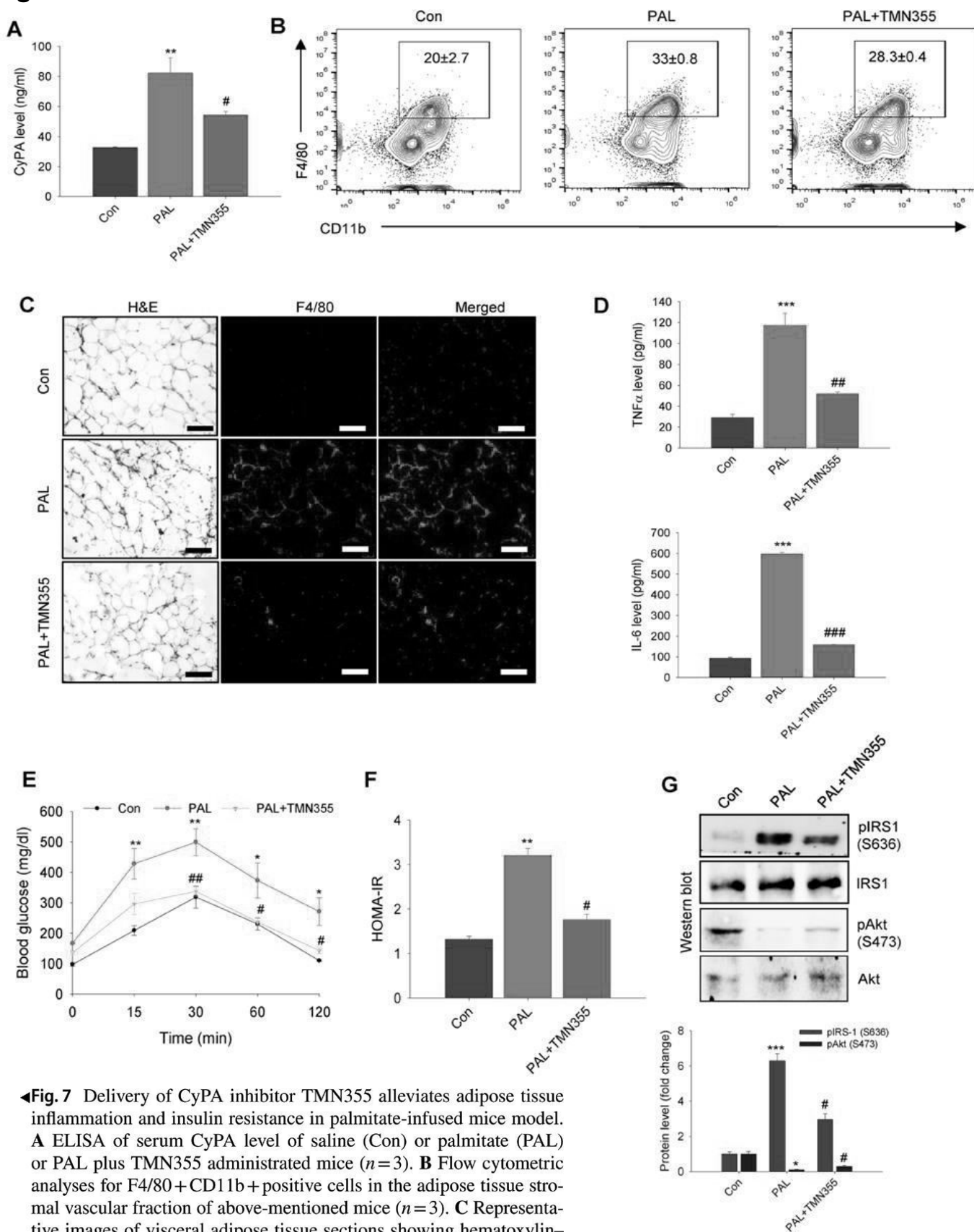


Fig. 6 CyPA-CD147-mediated NF- κ B activation impairs adipogenesis through β -catenin stabilization. **A** Real-time quantitative PCR analysis showing TNF- α , IL-1 β , PPAR- γ , and C/EBP- β mRNA level in 3T3-L1 adipocytes treated without or with CyPA (10 ng/ml) in the absence or presence of NF- κ B inhibitor Bay 11-7085 (20 μ M) for 8 h. β -Actin served as an internal control for normalization. **B** RT-PCR analysis (left) and its quantification (right) of PPAR- γ , C/EBP- β , TNF- α , and IL-1 β gene expressions in 3T3-L1 adipocytes treated without or with CyPA (10 ng/ml) in the absence or presence of Wnt signaling inhibitor IWR-1-endo (15 μ M) for 8 h. β -Actin was used as loading control. **C** Western blot images (upper) and its quantifications (lower) showing C/EBP- β and TNF- α abundance in 3T3-L1 adipocytes treated without or with CyPA (10 ng/ml) in the absence or presence of IWR-1-endo (15 μ M) for 8 h. **D** RT-PCR analysis (left) and its quantification (right) of LZTS2, Smurf1, and Smurf2 gene expressions in 3T3-L1 adipocytes treated without or with CyPA (10 ng/ml) in the absence or presence of Bay 11-7082 (20 μ M) or IWR-1-endo (15 μ M) for 8 h. β -Actin was used as loading control. All experiments were performed in triplicate. Each value is the mean \pm SEM of three independent experiments, *** p < 0.001, ** p < 0.01, * p < 0.05 vs Con; ### p < 0.001, ## p < 0.01, # p < 0.05 vs CyPA

Figure 7



◀**Fig. 7** Delivery of CyPA inhibitor TMN355 alleviates adipose tissue inflammation and insulin resistance in palmitate-infused mice model. **A** ELISA of serum CyPA level of saline (Con) or palmitate (PAL) or PAL plus TMN355 administrated mice ($n=3$). **B** Flow cytometric analyses for F4/80+CD11b+ positive cells in the adipose tissue stromal vascular fraction of above-mentioned mice ($n=3$). **C** Representative images of visceral adipose tissue sections showing hematoxylin-eosin staining along with the immunohistochemical analyses of F4/80 in saline (Con), palmitate (PAL) or PAL plus TMN355 administrated mice ($n=3$). Scale bar, 100 μ m. **D** Quantification of serum TNF α and IL-6 level in the above mice ($n=3$). **E**, **F** Glucose tolerance test (**E**) ($n=3$), and HOMA-IR analyses (**F**) ($n=3$) were performed in these mice. **G** Western blot images (upper) and its quantifications (lower) showing pIRS-1 (S636) and pAkt (S473) abundance in the adipose tissue of the above-mentioned mice ($n=3$). IRS-1 and Akt were used as loading control for normalization. *** $p < 0.001$, ** $p < 0.01$, * $p < 0.05$ vs Con; ### $p < 0.001$, ## $p < 0.01$, # $p < 0.05$ vs PAL

Figure 8

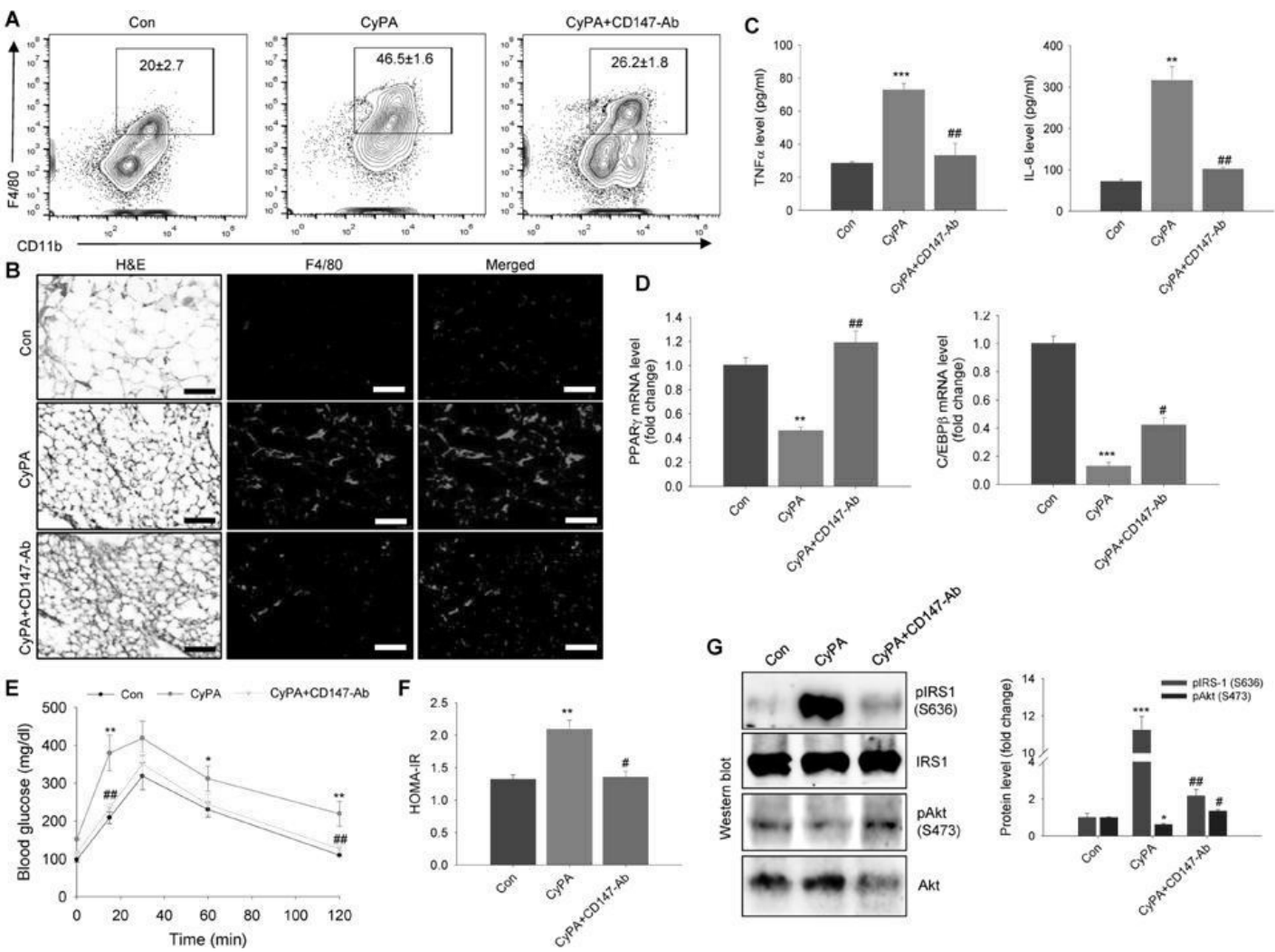


Fig. 8 Anti-CD147 antibody administration rescued CyPA-induced adipose tissue inflammation and insulin resistance in mice model. **A** Flow cytometric analyses for F4/80+CD11b+ positive cells in the adipose tissue stromal vascular fraction of saline (Con) or CyPA or CyPA plus anti-CD147 antibody (CD147-Ab) administrated mice ($n=3$). **B** Representative images of visceral adipose tissue sections showing hematoxylin–eosin staining along with the immunohistochemical analyses of F4/80 in Con or CyPA or CD147-Ab administrated mice ($n=3$). Scale bar, 100 μm . **C** Quantification of serum TNF α and IL-6 level in the above-mentioned mice ($n=3$). **D** Real-

time quantitative PCR analysis showing PPAR- γ , and C/EBP- β mRNA level in the visceral adipose tissue of these mice. β -Actin served as an internal control for normalization. **E**, **F** Glucose tolerance test (**E**), and HOMA-IR (**F**) analyses were performed in these mice ($n=3$). **G** Western blot images (left) and its quantifications (right) showing pIRS-1 (S636) and pAkt (S473) abundance in the adipose tissue of the above-mentioned mice ($n=3$). IRS-1 and Akt were used as loading control for normalization. *** $p < 0.001$, ** $p < 0.01$, * $p < 0.05$ vs Con; ## $p < 0.01$, # $p < 0.05$ vs CyPA

IIT Ropar:

Increased accumulation of body fat in obesity is considered the highest risk factor for the development of several metabolic diseases, including insulin resistance and type 2 diabetes. Excess storage of fat inside the adipocytes leads to the formation of hypertrophied adipocytes, which by releasing higher levels of circulatory free fatty acids, induce a state of chronic low-grade inflammation in adipocytes and adipose tissue macrophages (ATMs), resulting in the onset of obesity-induced adipose tissue inflammation. Obesity-induced enhancement of free fatty acids is accompanied by the reduction of adipose tissue vascularization, creating a zone deprived of adequate oxygen and nutrients. Accumulating evidence has revealed a considerable drop in pO₂, referred to as hypoxia in the subcutaneous and visceral adipose tissue (VAT) of obese patients with diabetes compared with lean subjects without diabetes. It has been shown that adipose tissue hypoxia plays a major role in adipose tissue inflammation and insulin resistance during the state of chronic obesity. Hypoxic adipocytes promote adipose tissue inflammation by secreting various proinflammatory cytokines and chemokines. The inflammatory chemokines, such as CCL2/MCP1, aggravate the adipose tissue inflammation by heightened infiltration of macrophages and its polarization toward the M1 phenotype, as evident in the obese adipose tissue of patients and mice. Although these studies have unveiled the significance of the obese adipose tissue microenvironment (ATenv) on inflammation and insulin resistance, the underlying mechanism is still elusive. Thus, it is important to elucidate how the hypoxic lipid-rich microenvironment in obese ATenv promotes adipose tissue inflammation and leads to the onset of insulin resistance.

Exploring the involvement of noncoding RNAs, particularly miRNAs, in obese hypoxic adipose tissue, it appears that miR-210 is a well-known hypoxia-inducible miRNA. Some evidence has shown that patients with diabetes, as well as diabetic animal models, have abnormally high levels of miR-210. In clinical studies, elevated levels of miR-210 have been detected in adolescent patients with type 1 diabetes and type 2 diabetes. Thus, we are interested in investigating any potential role of miR210-3p in ATMs for causing obesity-induced chronic lowgrade inflammation. Although the lone effects of palmitate or hypoxia on adipocyte function and insulin resistance have been well studied, the combined impact of high lipid content along with hypoxia on ATM inflammation is not clearly understood. In this study, we found that the obese hypoxic ATenv stimulates increased expression of miR-210-3p in the ATMs, provoking inflammation and polarization toward the M1 phenotype via the suppressor of cytokine signaling 1 (SOCS1)/nuclear factor-κB (NF-κB) pathway. Suppression of miR-210-3p markedly attenuated adipose tissue inflammation with improvement of insulin sensitivity. Therefore, targeting ATM-specific miR-210-3p could be an excellent strategy to regulate obesity-induced adipose tissue inflammation for the management of insulin resistance and type 2 diabetes.

By investigating the pathophysiological ATenv of the obese diabetic state, we found a marked induction of hypoxia and lipid accumulation in the VAT of obese patients type 2 diabetes and an HFD-induced obese diabetic mouse model as evident from hypoxia-inducible factor-1α (HIF-1α) levels (Fig. 1A and B) and lipid staining (Oil Red O and BODIPY F16) (Fig. 1A and B) compared with their control counterparts. This was further confirmed by the significant enhancement of triglyceride levels in the VAT of obese patients with diabetes and HFD mice (Fig. 1C) along with the lowering of oxygen tension indicated by Image-iT Green hypoxia staining in the VAT of HFD mice (Fig. 1D) compared with their respective controls. These results indicate the dyslipidemic and hypoxic state of the obese diabetic ATenv. We also noticed a significant accumulation of macrophage population in the VAT of obese patients with diabetes and HFD mice as indicated by CD68 and F4/80 staining (Fig. 1E and F). Since ATMs play a crucial role in obesity-associated chronic inflammation and insulin resistance, we were interested in exploring the involvement of specific miRNAs therein. To investigate the specific hypoxia-induced miRNAs in the ATMs of the obese diabetic ATenv, we searched existing

literature and considered a GEO database (GSE97652) that comprised an miRNA data set of ATM-derived exosomes (ATM-Exos) obtained from lean and obese mice. We reanalyzed the data set and filtered out the primary miRNAs associated with hypoxic conditions. Interestingly, the volcano plot derived from the DESeq2 analysis of the GSE97652 data set (Fig. 1G) showed six differentially expressed hypoxia-regulated miRNAs (miR-210-5p, miR-210-3p, miR-27a-5p, miR-27b-5p, miR-101b-5p, and miR-128-1-5p) in ATM-Exos of the obese mice compared with the lean controls. Figure 1H shows read count distribution box plots for these miRNAs in the ATM-Exos of lean and obese mice. Among these miRNAs, miR-210-3p exhibited maximum induction of an approximately fourfold increase in obese mice compared with lean controls. This finding led us to examine the miR-210-3p level in the ATMs of obese patients with diabetes and HFD mice. As expected, we observed a profound increase of miR-210-3p expression in ATMs isolated from the VAT of obese patients with diabetes and 12-week-old HFD mice compared with their respective controls (Fig. 1I and J). Taken together, these results demonstrate that a higher level of miR-210-3p is a key signature in the ATMs of the pathophysiological obese diabetic condition.

Since ATMs are the main source of inflammatory cytokine production in obesity-induced inflamed adipose tissue and cause its dysfunction, we explored how increased expression of miR-210-3p in obese ATEnv governs ATM inflammation and adipocyte dysfunction. We first set up an *in vitro* condition where RAW264.7 macrophages were coincubated with 1% O₂ and 0.75 mmol/L palmitate for various time periods to simulate the pathophysiological condition of obese ATEnv and analyzed miR-210-3p expression. H+L coexposure significantly increased miR-210-3p and HIF-1a levels at 16 h in RAW264.7 cells (Fig. 2A). Stimulation with hypoxia or lipid alone augmented miR-210-3p expression in macrophages, but the H+L coexposure potentiated miR-210-3p expression in macrophages to a greater extent (Fig. 2B). Moreover, H+L coexposure significantly stimulated gene expression of various proinflammatory cytokines (Fig. 2C) compared with the lone effect of hypoxia or lipid. Immunofluorescence staining of iNOS and ARG1 further confirmed that H+L coexposure caused iNOS levels to soar concomitant with the reduction of ARG1 levels in RAW264.7 macrophages (Fig. 2D and E). For a better understanding of the inflammatory nature of H+L -treated macrophages, we examined the expression profile of 21 different inflammatory genes and found a significant upregulation of NOS2, TNF- α , CXCL5, IL6, CCL2, IL1b, CD80, CD86, MHCII, and CCR2 gene expressions and downregulation of IL10, IL4, Ym1, CD206, and CD163 gene expressions (Fig. 2F), which depict the M1 macrophage phenotype. Furthermore, a significant enhancement of gene expression of proinflammatory cytokines was observed because of H+L in IL-4-induced M2 macrophages, suggesting an M2-to-M1 polarization shift. For more clarification, we have performed flow cytometric analysis of M1 (CD80) and M2 (CD206) phenotypic markers. All these results indicate that the obese hypoxic state of the ATEnv influences macrophages' M1 state with a higher level of miR-210-3p expression, suggesting a possible link of miR-210-3p with obesity-induced adipose tissue inflammation. To investigate the direct effect of miR-210 on macrophage M1 polarization and inflammation, RAW264.7 macrophages were transfected with miR-210-3p mimic or inhibitor in the absence and presence of an H+L microenvironment, followed by the analysis of M1/M2 populations through flow cytometry. Interestingly, miR-210-3p inhibition significantly reduced CD80 (M1) levels along with the induction of CD206 (M2) in H+L -treated macrophages (Fig. 2G). Concomitantly, we noticed suppression of proinflammatory cytokines genes (TNF- α , iNOS, and IL6) expression along with the upregulation of anti-inflammatory cytokines gene (IL4, IL13, and Ym1) expression in miR-210-3p-inhibited H+L -treated macrophages (Fig. 2H). ELISA further confirmed higher levels of IL-6 and TNF- α cytokine secretion from the H+L -stimulated macrophages, and this was significantly prevented in the presence of miR-210-3p inhibitor compared with the control inhibitor (Fig. 2I). Since miR-210-3p-inhibited macrophages were protected from H+L-induced inflammation, iNOS and ARG1 levels remained unaltered under the H+L microenvironment (Fig. 2J). On the contrary, introducing miR-210-3p mimic markedly upregulated the CD80 level in macrophages in the absence of H+L stimulation (Fig. 2K). Furthermore, induction of proinflammatory

TNF- α gene expression along with reduction of anti-inflammatory Ym1 gene expression (Fig. 2L) coincided with the increased levels of iNOS and subdued levels of ARG1 (Fig. 2M) observed in miR-210-3p mimic- transfected cells. Since obese adipose tissue had a profound accumulation of macrophages, which releases a considerable amount of miR-210-3p in the exosomes, we evaluated the impact of miR-210-3p in nearby adipocytes. These results revealed a direct role of miR-210-3p in ATM and adipocyte inflammation, favoring a state of inflamed adipose tissue that facilitates macrophage polarity switching toward the M1 proinflammatory phenotype.

To investigate the underlying mechanism of miR-210-3p involvement in obesity-induced ATM inflammation, we searched for the putative targets of miR-210-3p that can potentially regulate inflammatory pathways. We found that SOCS1 could be a potential target of miR-210-3p as indicated by the miRWalk miRNA target prediction database and that may be involved in the impairment of NF- κ B signaling. The nucleotide sequence of SOCS1 3' -UTR is conserved in the transcript sequence of humans and mice that critically offers the binding site of miR-210-3p (Fig. 3A). We used the RNAhybrid web server to predict the minimum free energy for the interaction of various SOCS1 mRNA transcripts with miR-210-3p. The miR-210-3p sequence complementary to the 3'-UTR of SOCS1 forms a hybrid sequence having a minimum free energy of 32.2 kcal/mol (mouse SOCS1 transcript) and 31.7 kcal/mol (human SOCS1 transcript). To validate the binding of miR-210-3p with the 3' -UTR of SOCS1, we performed a luciferase reporter assay with WT and mutant SOCS1 3'-UTR. H+L coexposure significantly inhibited luciferase activity in WT SOCS1 3' -UTR- transfected cells; however, such an effect was compromised in cells transfected with mutated SOCS1 3' -UTRs (Fig. 3B), indicating a direct interaction of miR-210-3p with the SOCS1 3' -UTR in the pathophysiological condition. We then examined SOCS1 expression and observed a significant reduction of its level in the stromal vascular fraction (SVF) of adipose tissue of obese patients with diabetes compared with lean participants without diabetes (Fig. 3C and D). Among the members of the SOCS family, only SOCS1 acts as a ubiquitin ligase that is capable of interacting with NF- κ B p65 through its SOCS box domain, which leads to polyubiquitination and proteasomal degradation of NF- κ B p65, resulting in termination of NF- κ B-inducible gene expression. We therefore analyzed the SOCS1-mediated NF- κ B activation in pathophysiological conditions. Western blot analysis showed a significant reduction of SOCS1 expression along with the enhanced levels of phosphorylated NF- κ B (pNF- κ B) in the adipose tissue SVF of obese patients with diabetes compared with lean participants without diabetes (Fig. 3E). To examine the role of macrophage-specific SOCS1 in macrophage inflammation, we silenced SOCS1 in RAW264.7 cells using siRNA and incubated them in the absence or presence of H+L stimulation. Silencing of SOCS1 significantly increased NF- κ B activation, whereas costimulation of H+L in SOCS1 silenced cells and further aggravated NF- κ B activation. Furthermore, to exclude the possibility of other targets of miR-210-3p that could contribute to the suppression of NF- κ B signaling, we analyzed RelA (p65 subunit of NF- κ B)-interacting partners using the EMBL INACT server. The RelA-interacting partners were searched against the 16,853 mmu-miR-210-3p target genes identified through the miRWALK database search, and BRD4, NF- κ B1B, SOCS1, CUL2, COMMD1, XPO1, and MYOCD were found to be predicted targets of mmu-miR-210-3p, of which SOCS1, NF- κ B1B, CUL2, COMMD1, and MYOCD are negative regulators of NF- κ B. To find out the most efficient target of miR-210-3p that can potentially inhibit NF- κ B under lipid-rich hypoxic conditions, we evaluated expression of these selected candidate genes in control mimic- and miR-210-3p mimic- transfected macrophages and observed a profound decline of SOCS1 gene expression (70%) compared with other candidate genes in miR-210-3p mimic-transfected cells. Also, we analyzed SOCS1 and NF- κ B activation in control and miR-210-3p inhibitor- transfected RAW264.7 macrophages cotreated with H+L. Exposure of H+L strikingly reduced SOCS1 expression, which coincided with the increased level of pNF- κ B and its nuclear translocation; however, such attributes were significantly attenuated in miR-210-3p inhibitor-transfected cells (Fig. 3F-H). Moreover, to assess whether the SOCS1 inhibitory effect on NF- κ B activation is mediated through the proteasomal degradation of pNF- κ B, we transfected macrophages with control or miR-210-3p inhibitor in the absence

or presence of the proteasome inhibitor MG-132 and treated with H+L. Our findings demonstrated that MG-132 treatment notably protects NF- κ B p65 phosphorylation-dependent proteasomal degradation in macrophages transfected with miR-210-3p inhibitor (Fig. 3I). Since the obesity-induced inflammatory milieu in adipose tissue is known to be associated with the impairment of insulin sensitivity (31), we cocultured 3T3-L1 adipocytes with macrophages transfected with a control inhibitor or miR-210-3p inhibitor in the absence or presence of H+L stimulation. Interestingly, attenuation of adipocytes' insulin sensitivity in response to its coculture with H+L-incubated macrophages was markedly prevented when transfected with miR-210-3p inhibitor (Fig. 3J). All these results suggest that miR-210-3p plays a key role in obesity-induced ATM inflammation by targeting the SOCS1/NF- κ B pathway and could also influence adipocytes' insulin sensitivity.

To inspect the therapeutic potential of miR-210-3p inhibitor in the rescue of obesity-induced adipose tissue inflammation and insulin resistance, we administered control LNA or anti-miR-210-3p LNA directly to the VAT of HFD mice (Fig. 4A). Also, we estimated the body weight and food intake for the entire 7 days of postsurgery to examine the postsurgery recovery of mice. On day 7, adipose tissue was harvested for immunofluorescence analysis of F4/80, CD163, iNOS, and ARG1. A profound increase in the anti-inflammatory CD163+ F4/80+ macrophage population was observed in the HFD adipose tissue injected with anti-miR-210-3p LNA (Fig. 4B). Similarly, a reduced level of iNOS and an enhanced level of ARG1 were also seen in the anti-miR-210-3p LNA adipose tissue of HFD mice (Fig. 4C). Moreover, we collected the ATMs from these mice on day 7 and analyzed for ATM polarization and inflammation. HFD mice administered anti-miR-210-3p LNA exhibited an abundance of the M2 (F4/80+CD206+) over the M1 (F4/80+CD80+) ATM population (Fig. 4D), with a notable reduction of proinflammatory (iNOS, IL6) over anti-inflammatory (IL13, Ym1) cytokine gene expression (Fig. 4E) compared with control LNA-injected HFD mice. To exclude the contributions of other cell types in adipose tissue in response to anti-miR-210-3p LNA treatment, we checked miR-210-3p and SOCS1 expression in the adipocytes isolated from mice injected with control LNA and anti-miR-210-3p LNA. We found that miR-210-3p expression was reduced in isolated adipocytes of mice administered anti-miR-210-3p LNA, but not significantly compared with controls. These results suggest that adipocytes' contribution has not been substantial for altering the adipose tissue inflammatory state upon anti-miR-210-3p LNA treatment; rather, it depicts the exclusive role of miR-210-3p in ATM inflammation, and, therefore, ATM-specific inhibition of miR-210-3p would be beneficial to improve the inflammatory setting of obese adipose tissue. As we found that miR-210-3p promotes NF- κ B activation-dependent inflammation in RAW264.7 macrophages by targeting the SOCS1/NF- κ B pathway (Fig. 3), we examined the level of SOCS1 expression and NF- κ B activation in the adipose tissue of standard diet and HFD mice treated with control LNA or anti-miR-210-3p LNA. Immunofluorescence analysis showed a profound induction of SOCS1 in the VAT of HFD mice treated with anti-miR-210-3p LNA (Fig. 4F). Upregulation of SOCS1 expression (Fig. 4G and H) coincided with the subdued levels of pNF- κ B p65 (Fig. 4H) in the ATMs of HFD mice administered anti-miR-210-3p LNA. Moreover, by investigating the insulin sensitivity of HFD mice treated with control LNA or anti-miR-210-3p LNA, we found that anti-miR-210-3p LNA delivery significantly restored HFD mice from diet-induced insulin resistance as indicated by glucose tolerance test (Fig. 4I), insulin tolerance test (Fig. 4J), and HOMA of insulin resistance (Fig. 4K). These results suggest that the application of anti-miR-210-3p LNA could be beneficial in rescuing obesity-induced inflammation and insulin resistance.

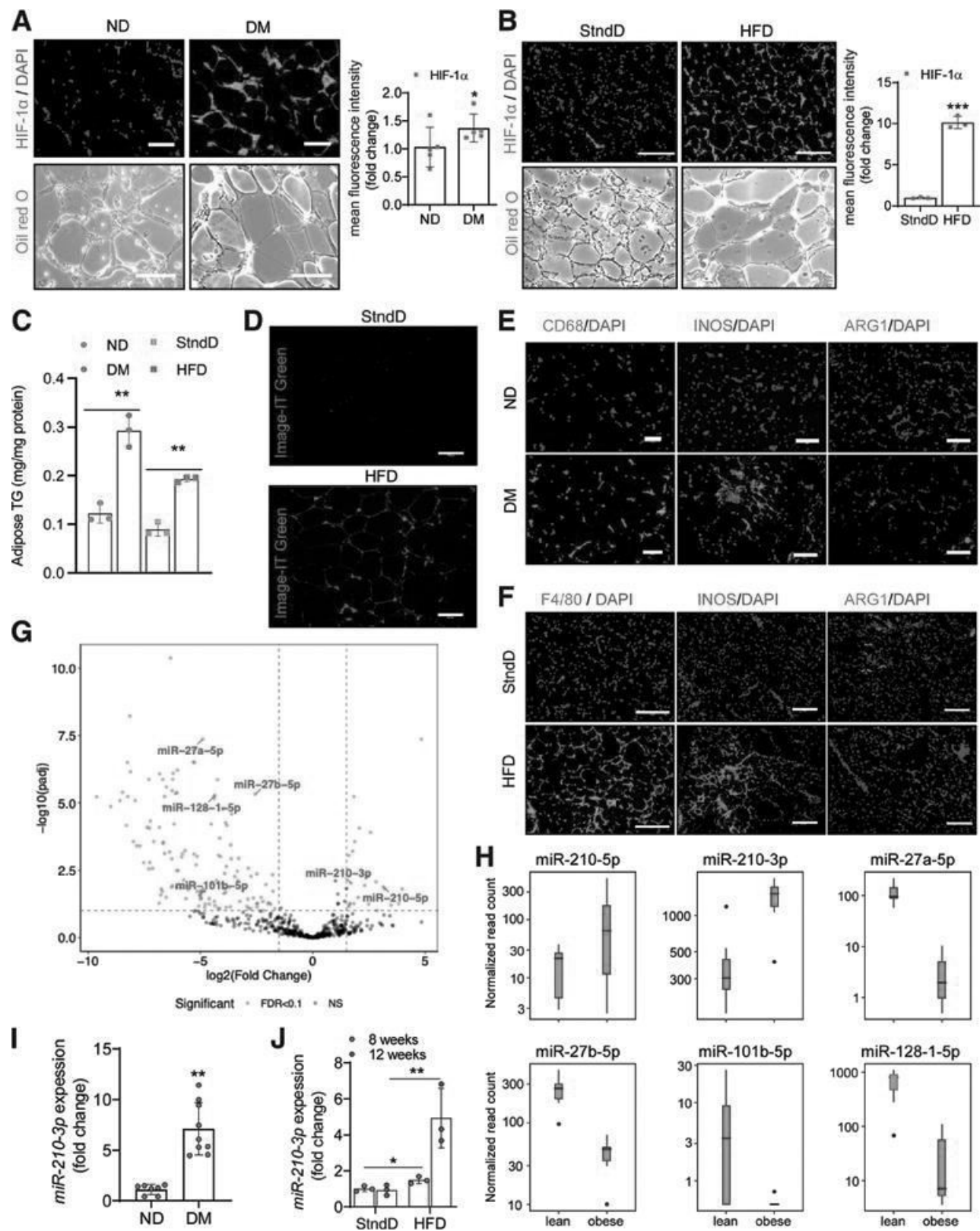
Figure 1

Figure 1—Lipid-rich low oxygen tension in obese ATenv potentiates high *miR-210-3p* expression in ATMs. **A** and **B**: Representative images of human (scale bar = 100 μ m, n = 5) (**A**) and mouse (scale bar = 200 μ m, n = 3) (**B**) VAT sections with HIF-1 α immunohistochemical staining or Oil Red O staining with quantification data. * P < 0.05, *** P < 0.001 (Student t test). **C**: VAT triglyceride (TG) level was measured in nonobese participants without diabetes (ND) and obese patients with diabetes (DM) and mice fed a standard diet (StdD) and HFD. ** P < 0.01. **D**: Image-IT Green hypoxia staining of VAT sections of StdD and HFD mice (scale bar = 100 μ m). **E**: Immunohistochemical analysis of CD68, iNOS, and ARG1, in VAT from ND and DM group participants (scale bar = 100 μ m). **F**: Representative images of StdD and HFD mouse VAT sections with F4/80, iNOS, and ARG1 immunohistochemical staining (scale bar = 200 μ m). **G**: Volcano plot derived from the DESeq2 analysis of the GSE97652 data set indicates that miRNAs are differentially expressed between obese and lean samples. The y -axis denotes $-\log_{10}$ of P -adjusted (padj) values obtained from the DESeq2 pipeline, and \log_2 fold change is plotted on the x -axis. Red dots indicate significant miRNAs that passed certain criteria filters (false discovery rate [FDR] < 0.1, $|\log_2$ fold change| > 1.5), while black dots are considered nonsignificant. Annotated miRNAs with purple text are of special interest. **H**: Read count distribution box plots for five miRNAs of interest overlapped with differentially expressed miRNAs. The y -axis indicates normalized read counts on the \log_{10} scale. The x -axis indicates two different levels of conditions for mice. **I**: Quantitative RT-PCR analyses of *miR-210-3p* in ATMs of the ND and DM group participants (n = 7–9). ** P < 0.01 (Student t test). **J**: Relative expression of *miR-210-3p* in F4/80⁺-sorted ATMs from VAT from StdD and HFD mice at 8 weeks and 12 weeks (n = 3). * P < 0.05, ** P < 0.01 (Student t test). Data are mean \pm SD.

Figure 2

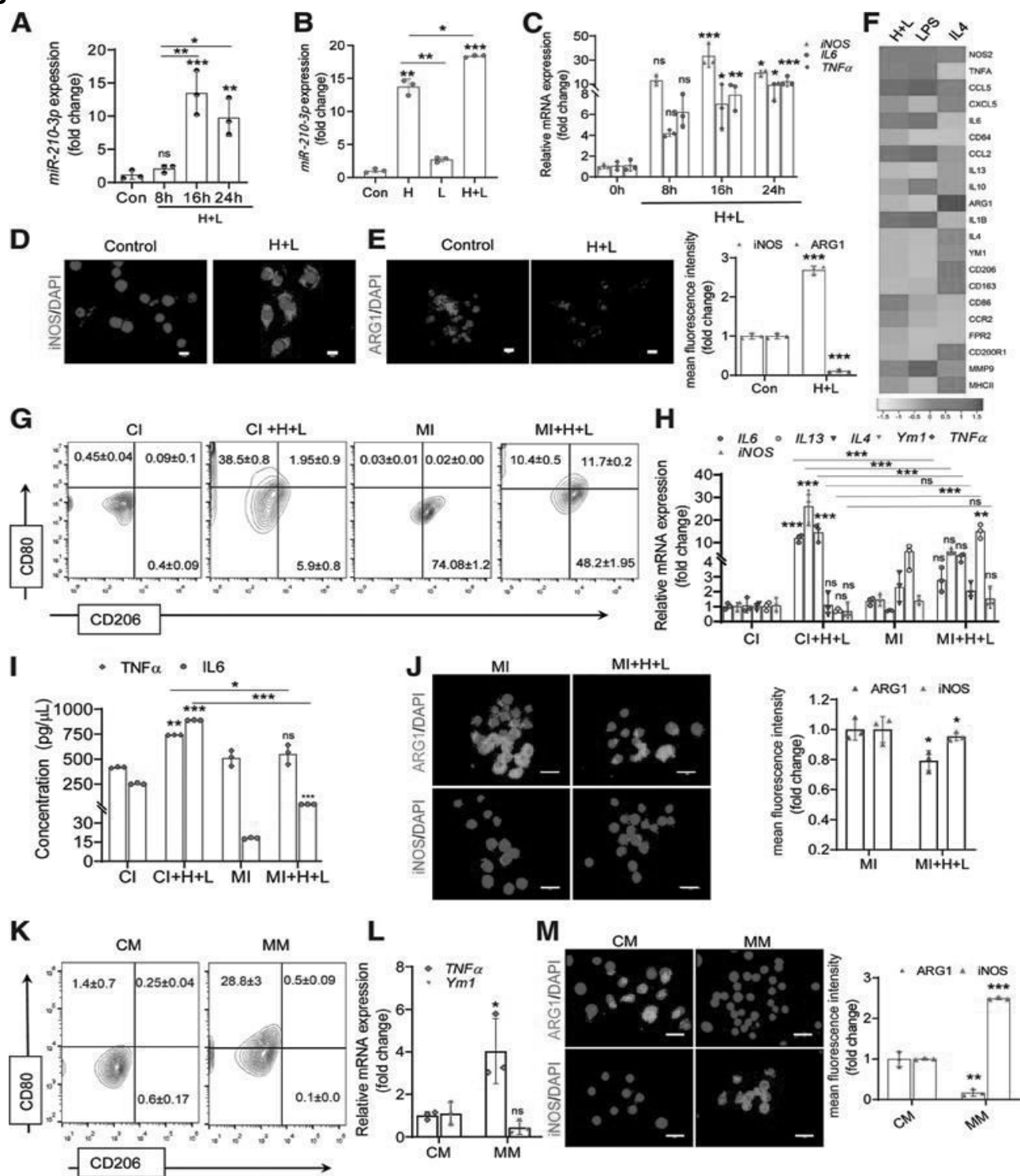


Figure 2—Chronic obese ATenv promotes ATM skewing toward M1. **A** and **B**: Quantitative RT-PCR analyses of *miR-210-3p* expression in RAW264.7 murine macrophages, coincubated with H + L for various time periods (**A**) and treated with hypoxia or lipid alone or in combination for 16 h (**B**) ($n = 3$). * $P < 0.05$, ** $P < 0.01$, *** $P < 0.001$ by one-way ANOVA. **C**: Relative mRNA expression of proinflammatory cytokines *iNOS*, *IL6*, and *TNF- α* in H + L-costimulated macrophages for various time periods (8, 16, and 24 h) ($n = 3$). * $P < 0.05$, ** $P < 0.01$, *** $P < 0.001$ by one-way ANOVA. **D** and **E**: Immunofluorescence analysis of *iNOS* (**D**) and *ARG1* (**E**) expression with quantification analyses in murine macrophages cotreated with or without H + L. DAPI was used for nuclear staining (scale bar = 10 μm , $n = 3$). *** $P < 0.001$ by Student *t* test. **F**: Quantitative RT-PCR analyses of various proinflammatory and anti-inflammatory markers in H + L-treated macrophages for 16 h. Lipopolysaccharide (LPS) and IL-4 treatment were considered as positive control for M1 and M2 phenotype macrophages, respectively. **G**: Flow cytometry analyses for CD80 and CD206 in control inhibitor (CI)- or *miR-210-3p* inhibitor (MI)-treated mouse macrophages coincubated with or without H + L ($n = 3$). **H**: Quantitative RT-PCR analyses of proinflammatory cytokines (*iNOS*, *TNF- α* , *IL6*) and anti-inflammatory cytokines (*Ym1*, *IL4*, *IL13*) in CI- or MI-treated mouse macrophages coincubated with or without H + L ($n = 3$). ** $P < 0.01$, *** $P < 0.001$ by two-way ANOVA. **I**: Quantification of extracellular release of *IL-6* and *TNF- α* in CI- or MI-treated mouse macrophages coincubated with or without H + L ($n = 3$). * $P < 0.05$, ** $P < 0.01$, *** $P < 0.001$ by two-way ANOVA. **J**: Immunofluorescence analysis of *iNOS* and *ARG1* expression in MI-treated macrophages coincubated with or without H + L and quantification analyses. DAPI was used for nuclear staining (scale bar = 20 μm , $n = 3$). * $P < 0.05$ by Student *t* test. **K**: Flow cytometry analyses for CD80 and CD206 in control mimic (CM)- or *miR-210-3p* mimic (MM)-treated macrophages. **L**: Relative gene expression of *TNF- α* and *Ym1* in CM- or MM-treated macrophages ($n = 3$). * $P < 0.05$ by Student *t* test. **M**: Immunofluorescence analysis of *iNOS* and *ARG1* expression in CM- or MM-treated macrophages and quantification analyses. DAPI was used for nuclear staining (scale bar = 20 μm , $n = 3$). ** $P < 0.01$, *** $P < 0.001$ by Student *t* test. Data are mean \pm SD. Con, control.

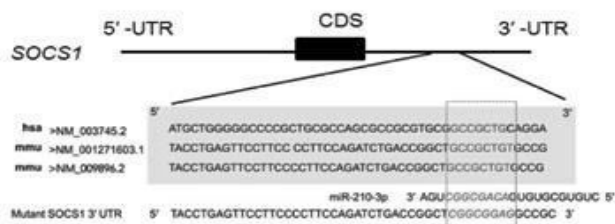
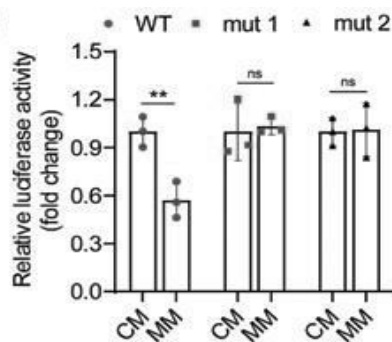
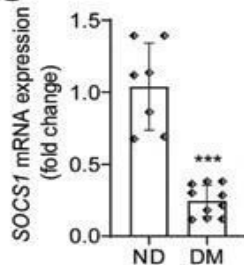
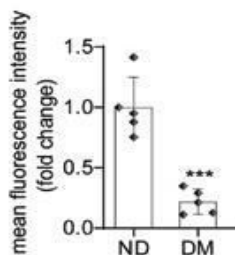
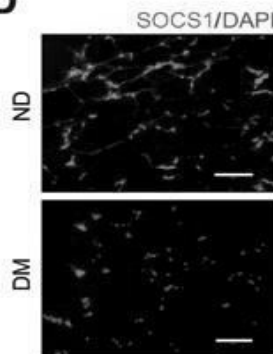
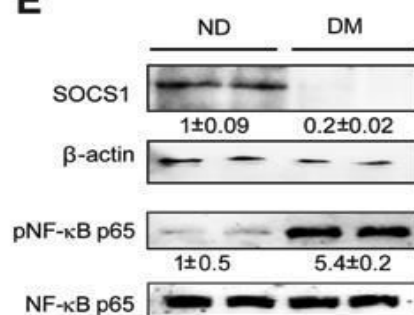
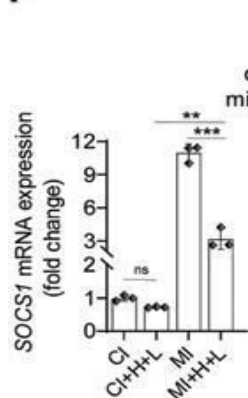
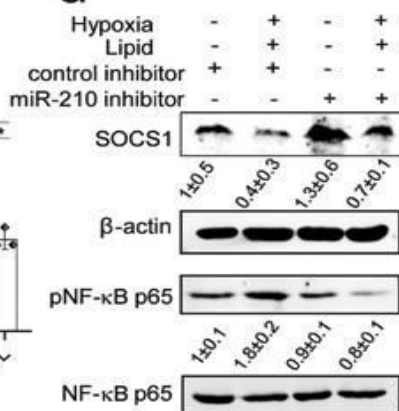
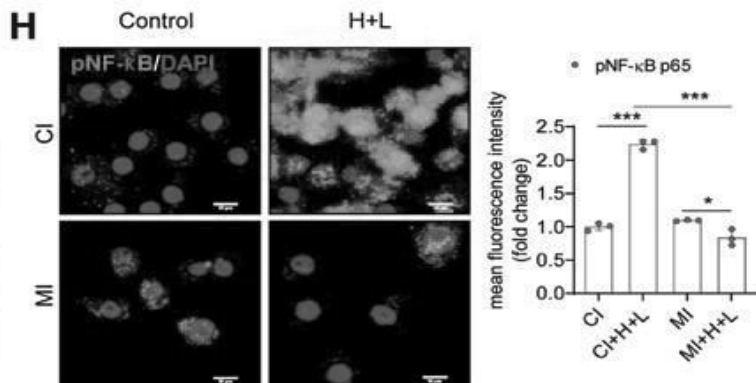
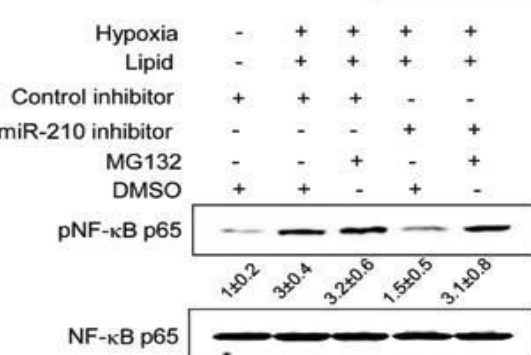
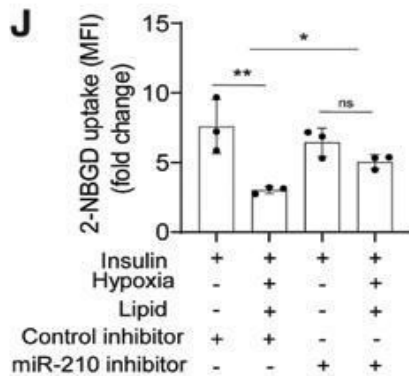
Figure 3**A****B****C****D****E****F****G****H****I****J**

Figure 3—miR-210-3p derives obesity-induced ATM polarization and inflammation by targeting the SOCS1-NF-κB pathway. **A:** Putative conserved binding site of *SOCS1* with *miR-210-3p* and seed sequence of *miR-210-3p* and mutated 3'-UTR site of *SOCS1*. **B:** Luciferase activity in RAW264.7 macrophages cotransfected with WT or mutated (mut1 and mut 2) *SOCS1* plasmid constructs and control mimic (CM) or *miR-210-3p* mimic (MM) ($n = 3$). ** $P < 0.01$ by Student t test. **C:** Relative mRNA expression of *SOCS1* in SVFs of nonobese participants without diabetes (ND) and obese patients with diabetes (DM) ($n = 7-10$). *** $P < 0.001$ by Student t test. **D:** Immunohistochemical staining of *SOCS1* in adipose tissue section of human VAT and quantification analyses (scale bar = 100 μm , $n = 5$). *** $P < 0.001$ by Student t test. **E:** Western blot analyses of *SOCS1* and pNF- κB in the cellular lysate of SVFs isolated from VAT of the ND and DM participant groups. **F-G:** Control inhibitor (CI)- or *miR-210-3p* inhibitor (MI)-treated macrophages coincubated with or without H + L considered for mRNA expression analyses of *SOCS1* (**F**) and Western blot analyses of *SOCS1* and pNF- κB p65 (**G**). ($n = 3$) ** $P < 0.01$, *** $P < 0.001$ by one-way ANOVA. **H:** Immunofluorescence analysis showing nuclear localization and expression of pNF- κB in CI- or MI-treated macrophages coincubated with or without H + L and quantification analyses (scale bar = 10 μm , $n = 3$). * $P < 0.05$, *** $P < 0.001$ by one-way ANOVA. **I:** Immunoblotting analyses of pNF- κB in CI and MI macrophages treated with or without H + L and MG-132. DMSO was used as vehicle control. **J:** Glucose uptake assay performed in 3T3-L1 adipocytes cocultured (transwell) with CI- or MI-transfected macrophages in the presence or absence of H + L ($n = 3$). * $P < 0.05$, ** $P < 0.01$ by one-way ANOVA. Data are mean \pm SD. CDS, coding sequence; MFI, mean fluorescence intensity.

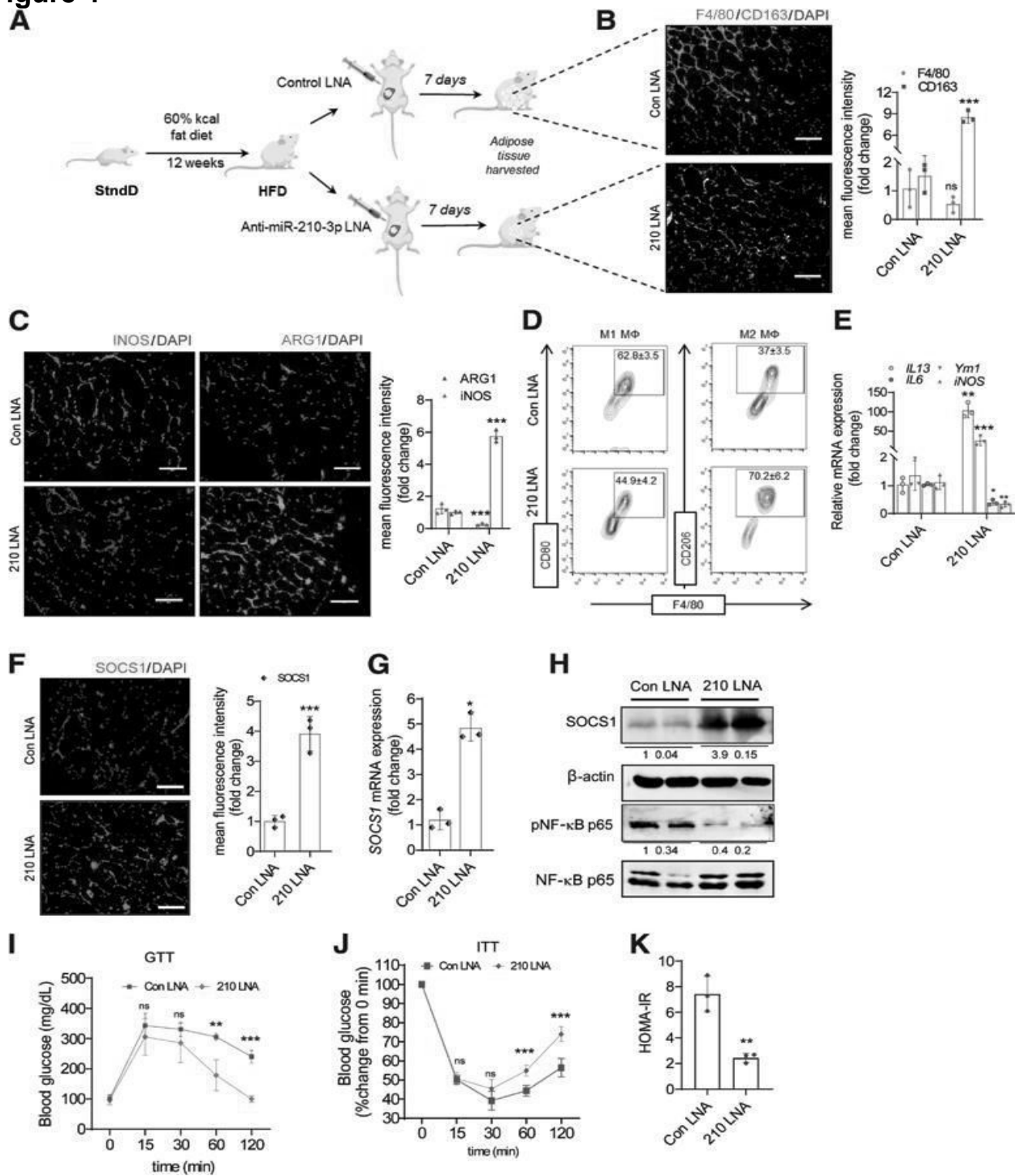
Figure 4

Figure 4—Anti-*miR*-210-3p LNA delivery rescues obesity-induced ATM inflammation and insulin resistance. **A:** Schematic diagram showing the development of the HFD (diet-induced obesity) mouse model and adipose tissue-specific delivery of control LNA or anti-*miR*-210-3p LNA. **B** and **C:** Representative images of VAT sections showing immunohistochemical staining along with quantification analyses of F4/80 and CD163 (**B**) or iNOS and ARG1 (**C**) in HFD mice injected with control LNA and anti-*miR*-210-3p LNA (scale bar = 200 μ m, n = 3). *** P < 0.001 by Student t test. **D:** Flow cytometry analyses for F4/80⁺CD80⁺ and F4/80⁺CD206⁺ cells in the SVF of HFD mouse VAT injected with control LNA or anti-*miR*-210-3p LNA (n = 3). ** P < 0.01, *** P < 0.001. **E:** Relative gene expression of proinflammatory cytokines (*IL6*, *iNOS*) and anti-inflammatory cytokine (*IL13*, *Ym1*) in sorted ATMs from HFD mice injected with control LNA or anti-*miR*-210-3p LNA (n = 3). * P < 0.05, ** P < 0.01, *** P < 0.001 by Student t test. **F:** SOCS1 protein expression was analyzed and quantified by performing immunohistochemical staining of VAT of HFD mice injected with control LNA or anti-*miR*-210-3p LNA with quantification analyses (scale bar, 200 μ m, n = 3). *** P < 0.001 by Student t test. **G:** Quantitative RT-PCR analyses of SOCS1 mRNA in the ATMs of HFD mice injected with control LNA or anti-*miR*-210-3p LNA (n = 3). * P < 0.05 by Student t test. **H:** Western blot analysis was performed to measure pNF- κ B and SOCS1 protein expression in the ATMs of HFD mice injected with control LNA or anti-*miR*-210-3p LNA. **I–K:** Glucose tolerance test (GTT) (**I**), insulin tolerance test (ITT) (**J**), and HOMA of insulin resistance (HOMA-IR) (**K**) analyses were performed in HFD mice injected with control LNA or anti-*miR*-210-3p LNA (n = 3). ** P < 0.01, *** P < 0.001 by two-way ANOVA. Data are mean \pm SD. 210, anti-*miR*-210-3p; Con, control; StndD, standard diet.

B2: Summary and Conclusions:

Tezpur University:

We provide evidence that a lipid-induced monokine cyclophilin-A (CyPA) significantly attenuates adipocyte functions and insulin sensitivity. Targeted inhibition of CyPA in diet-induced obese zebrafish notably reduced adipose tissue inflammation and restored adipocyte function resulting in improvement of insulin sensitivity. Silencing of macrophage CyPA or its pharmacological inhibition by TMN355 effectively restored adipocytes' functions and insulin sensitivity. Interestingly, CyPA incubation markedly increased adipocyte inflammation along with an impairment of adipogenesis, however, mutation of its cognate receptor CD147 at P309A and G310A significantly waived CyPA's effect on adipocyte inflammation and its differentiation. Mechanistically, CyPA-CD147 interaction activates NF- κ B signaling which promotes adipocyte inflammation by upregulating various pro-inflammatory cytokines gene expression and attenuates adipocyte differentiation by inhibiting PPAR γ and C/EBP β expression via LZTS2-mediated downregulation of β -catenin. Moreover, inhibition of CyPA or its receptor CD147 notably restored palmitate or CyPA-induced adipose tissue dysfunctions and insulin sensitivity. All these results indicate that obesity-induced macrophage-adipocyte cross-talk involving CyPA-CD147 could be a novel target for the management of insulin resistance and type 2 diabetes.

IIT Ropar:

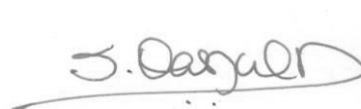
We have shown that hypoxia and lipid (HL) surge synergistically foster adipose tissue macrophage (ATM) inflammation and its polarization. HL co-exposure markedly increased miR-210-3p expression in macrophages which promotes NF- κ B activation-dependent pro-inflammatory cytokines expressions along with the downregulation of anti-inflammatory cytokines expression. Interestingly, delivery of miR-210-3p mimic significantly increased the macrophage inflammation in absence of HL co-stimulation; while miR-210-3p inhibitor delivery notably compromised HL-induced macrophage inflammation through increased production of SOCS1, a negative regulator of NF- κ B inflammatory signalling pathway. Mechanistically, miR-210 directly binds to 3'UTR of SOCS1 mRNA and silenced its expression and thus preventing proteasomal degradation of NF- κ B p65. Direct delivery of anti-miR-210-3p LNA in the adipose tissue markedly rescued mice from obesity-induced adipose tissue inflammation and insulin resistance. Thus, miR-210-3p inhibition in ATMs could serve as a novel therapeutic strategy for managing obesity-induced type 2 diabetes.

B3. Details of New Leads Obtained, if any:

- (i) We have identified a lipid-induced monokine CyPA which play a critical role in obesity-induced macrophage-adipocyte cross-talk and insulin resistance. Thus, CyPA-CD147 could be a novel target for the management of insulin resistance and type 2 diabetes.
- (ii) We discover that co-exposure of hypoxia and lipid (H+L) markedly increased miR-210-3p expression in macrophages which promotes pro-inflammatory state and insulin resistance. Thus, miR-210-3p inhibition in ATMs could serve as a novel therapeutic strategy for managing obesity-induced type 2 diabetes

B4. Details of Publications & Patents, if any:

1. D. Banerjee, D. Patra, A. Sinha, S. Roy, R. Pant, R. Sarmah, R. Dutta, S. K. Bhagabati, K. Tikoo, **D. Pal, S. Dasgupta** (2022) Lipid-induced monokine Cyclophilin-A promotes adipose tissue dysfunction implementing insulin resistance and type 2 diabetes in zebrafish and mice models of obesity. **Cellular and Molecular Life Sciences 79, 282** [DOI: 10.1007/s00018-022-04306-1] **(IF: 9.207)**
2. D. Patra, S. Roy, L. Arora, S. W. Kabeer, S. Singh, U. Dey, D. Banerjee, A. Sinha, **S. Dasgupta**, K. Tikoo, A. Kumar, **D. Pal** (2022) miR-210-3p promotes obesity-induced adipose tissue inflammation and insulin resistance by targeting SOCS1 mediated NF- κ B pathway. **Diabetes** [Accepted on November 29, 2022] **(IF: 9.332)**



[Signature(s) of the Investigator(s)]

Instructions:

- (i) *All the information needs to be provided; otherwise the Progress Report will be treated as incomplete. In case of 'Nil' / 'Not Applicable' information, the same may be indicated.*
- (ii) *In case of multicentre project, a combined Progress Report should be submitted incorporating the progress of all components. The Project Co-coordinator/ PI will be responsible for this.*
- (iii) **Please indicate the reporting period [i.e. Year 1/2/3/4/5].*
- (iv) *Submission of Progress Report by the end of the 11th month of grant sanction is linked with further continuation of the project and timely release of funds for the next year.*

UTILISATION CERTIFICATE
(For the financial 1st April to 25th June 2022)

(Rs. In lakhs)

1. Title of the project/scheme :
"Understanding the role of adipose tissue remodelling in exercise induced insulin sensitivity"
2. Name of the Organisation : Tezpur University
3. Principal Investigator : Dr. Suman Dasgupta
4. Deptt. of Biotechnology sanction order No. :
BT/PR24700/NER/95/819/2017
& date of sanctioning the project Dated: 26/06/2018
5. Amount brought forward from the previous financial year quoting DBT sanction No. & date in which the authority to carry forward the said amount was given : Rs. 0.73084
6. Amount received from DBT during the financial year (Please give No. & dates of Sanction order showing the amounts) : Nil
7. Other receipts/interest earned, if any, : 0.00242
8. Total amount that was available for expenditure during the financial year (Sl. Nos. 2 and 3) : Rs. 0.73326
9. Actual expenditure (excluding commitments) : Rs. 0.58559
Incurred during the financial year
(Statement of Expenditure is enclosed)
10. Unspent balance refunded, if any (Please give the details of Cheque No. etc.) : Nil
11. Balance amount available at the end of the financial year :Rs. 0.14767
12. Amount allowed to be carried forward to the Next financial year vide letter No. & date : Nil

1. Certified that the amount of **Rs.0.58559lakhs** mentioned against col. 5 has been utilized on the project/ scheme for the purpose for which it was sanctioned and that the balance of **Rs. 0.14767lakhs** remaining unutilized at the end of the year has ~~been surrendered to Govt.~~ (Vide No. dated) will be adjusted towards the grants-in-aid payable during the next year.

2. Certified that I have satisfied myself that the conditions on which the grants-in-aid was sanctioned have been duly fulfilled/are being fulfilled and that I have exercised the following checks to see that the money was actually utilized for the purpose for which sanctioned.

Kinds of checks exercised:

- 1.Rs. 0.53865 lakhs for consumables
2. Rs. 0.02911 lakhs for Travel



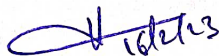
(PROJECT INVESTIGATOR)

Dr. S. Dasgupta
PI, DBT- Twinning Project
DBT Ref. No.: BT/PR24700/NER/95/819/2017
Univ. ref. No: DoRD/MBBT/SD/20-382
Dept. of MBBT, Tezpur University
Assam- 784028, INDIA



(FINANCE OFFICER)

Finance Officer
Tezpur University



(HEAD OF THE INSTITUTE)

Registrar
Tezpur University

(To be countersigned by the DBT Officer-in-charge)

Annexure II

STATEMENT OF EXPENDITURE REFERRED TO IN PARA 9 OF THE UTILISATION CERTIFICATE
Showing grants received from the Department of Biotechnology and the expenditure incurred during the period
from 1st April 2022 to 25th June 2022.

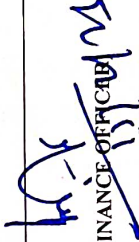
(Rs. In lakhs)

Item	Unspent balance carried forward from previous year	Grants received from DBT during the year/ Interest earned	Total of Col. (2+3)	Expenditure (excluding commitments incurred during the year)	Balance (4-5)	Remarks
	2	3	4	5	6	
1. Non-Recurring i) Equipment's	Nil	Nil	Nil	Nil	Nil	
2. Recurring (i) Human Resource	Rs. 0.04643	Nil	Rs. 0.04643	Nil	Rs. 0.04643	
(ii) Consumables	Rs. 0.20043	Nil	Rs. 0.20043	Rs. 0.53865	Rs. -0.33822	
(iii) Travel	Rs. 0.00910	Nil	Rs. 0.00910	Rs. 0.02911	Rs. -0.02001	
(iv) Contingency	Rs. 0.29199	Nil	Rs. 0.29199	Rs. 0.29199	Rs. 0.00000	
(v) Overhead (If applicable)	Rs. 0.16506	Nil	Rs. 0.16506	Nil	Rs. 0.16506	
(vi) Interest earned	0.01783	0.00242	Rs 0.02025	0.01783	0.00242	0.01783 Interest refunded in Bharat Kosh Transaction ID: 2605220007965 dated 31 st May, 2022
Total	Rs. 0.73084	0.00242	Rs. 0.73326	Rs. 0.58559	Rs. 0.14767	

S. Dasgupta
(PROJECT INVESTIGATOR PI, DBT- Twinning Project)
DBT Ref. No.: BT/PR24700/NERJ5/19/2017
Univ. ref. No: DORC/MBBT/SD/20-382
Dept. of MBBT, Tezpur University
Assam- 784028, INDIA


(HEAD OF THE INSTITUTE)
Registrar

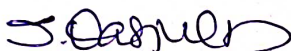
Tezpur University


(FINANCE OFFICER)
Finance Officer
Tezpur University

Annexure A

Manpower Staffing Details for the DBT-Twinning project sanctioned by
the Department of Biotechnology (during the period
from 1st April 2022 to 25th June 2022

NAME OF THE PERSON	NAME OF THE POST	DATE OF JOINING	DATE OF LEAVING	TOTAL MONTHLY SALARY	TOTAL SALARY PAID	TOTAL SALARY PAID DURING PROJECT PERIOD
Dipanjana Banerjee	JRF	01/10/2018	-	Rs 31,000	Nil	Rs 7,57,000



(Signature of Principal Investigator)

Dr. S. Dasgupta
PI, DBT- Twinning Project
DBT Ref. No.: BT/PR24700/NER/95/819/2017
Univ. ref. No: DoRC/MBBT/SD/20-382
Dept. of MBBT, Tezpur University
Assam- 784028, INDIA



(Signature of Accounts Officer)

Finance Officer
Tezpur University



(SIGNATURE OF HEAD OF THE INSTITUTE)

Registrar
Tezpur University

Manpower Expenditure Details (In financial year wise manner)*:

SANCTIONED POSTS	NUMBER	SCALE OF PAY	ANNUAL OUTLAY	OUTLAY FOR THE ENTIRE PERIOD	REVISED SCALE, IF ANY	REVISED ANNUAL OUTLAY	REVISED PROJECT OUTLAY	ACTUAL RELEASES BY DBT	ACTUAL EXPENDITURE	BALANCE
JRF: For First & Second Year SRF: For Third Year	Two(2)	First Two Years: Rs.25,000 + Rs. 2500 (HRA) = Rs.27,500 Third Year: Rs. 28,000 + Rs.2800 (HRA)= Rs. 30,800	First Two Years: Rs. 6,60,000 Third Year: Rs. 3,69,996	Rs. 10,29,996	Rs. 31,000 (JRF) Rs.35,000 (SRF)	Rs.12,40,800	Rs.7,61,643	Rs. 7,61,643	Rs. 7,57,000	Rs. 4,643

(Signature of Principal Investigator)

Dr. S. Dasgupta

PI, DBT- Twinning Project
DBT Ref. No.: BT/PR24700/NER/95/819/2017
Univ. ref. No: DoRC/MBBT/SD/20-382
Dept. of MBBT, Tezpur University
Assam- 784028, INDIA

(Signature of Accounts Officer)

Finance Officer
Tezpur University

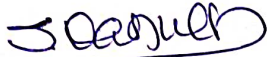
(SIGNATURE OF HEAD OF THE INSTITUTE)

Registrar
Tezpur University

* Details of manpower salary/ fellowship revision alongwith due- drawn statement and arrears requested should be given separately, if applicable.

Due- Drawn Statement

Name of the Project Staff	Month and Year	Due	Drawn	Difference
Dipanjan Banerjee	April,2018	31,000	Nil	31,000
	May,2018	31,000	Nil	31,000
	June,2018	31,000	Nil	31,000



(Signature of Principal Investigator)

Dr. S. Dasgupta

PI, DBT- Twinning Project

DBT Ref. No.: BT/PR24700/NER/95/819/2017

Univ. ref. No: DoRC/MBBT/SD/20-382

Dept. of MBBT, Tezpur University

Assam- 784028, INDIA


(Signature of Accounts Officer)

Finance Officer
Tezpur University


(SIGNATURE OF HEAD OF THE INSTITUTE)

Registrar
Tezpur University